NTNU – Trondheim
Norwegian University of
Science and Technology

Numerical modelling of a Czochralski furnace with active cooling jacket

Optimization of quality and througput

Zhengyu Li

Light Metals, Silicon and Ferroalloy Production
Submission date: Januar 2015
Supervisor: Eivind Øvrelid, IMTE
Co-supervisor: Martin Bellmann, Sintef

Norwegian University of Science and Technology
Department of Materials Science and Engineering

Abstract

In the single crystal silicon Czochlarski process, pull rate has a great impact on its production. More and more people put their eyes on optimizing the structure of Cz furnace to increase the pull rate, but experiments require a lot of capital to support. Due to the high cost and risk of crystal growth experiments, numerical simulation of Cz process becomes highly used as an effective tool to improve the structure of furnace and analysis the mechanism during the process. Based on a SINTEF Cz furnace, we wanted to investigate the possibility to install a cooling jacket around crystal to improve the crystallization. By comparing the numerical results before and after installing the cooling jacket, it was found that the new cases shows a satisfied conclusion on improving the pull rate and reducing the power consumption.

Contents

Chapter 1 Introduction

1 PV industry

Solar is a kind of inexhaustible, free and clean energy as known all over the world. It is predicted that solar photovoltaic power generation will occupies an important position in the 21st century, it will not only replace a part of traditional energy sources, but also become the main part of the world's energy consumption. It is expected that solar power will account for more than 20% in the total electricity supply by 2040 and this data will become 60% in the end of this century. These figures are fairly enough to show the development prospects of solar photovoltaic industry and important position in world's energy sources.

Early in 1839, Edmund Becquerel [1] discovered photovoltaic effect. After a century, Daryl Chapin, Calvin Fuller and Gerald Pearson [2] produced the first silicon substrate cell in Bell laboratory, which means that the photovoltaic technology had a new start.

After 1970s, with the development of modern industry, the global energy crisis and air pollution problems have revealed increasingly. At this time, the whole world put their target into renewable energy, they hoped that renewable energy can make the energy mix to a sustainable development. On this issue, solar energy got people's attention because of its unique advantages. After 1980s, the type of solar cell is growing, the range of applications are increasing and the scale of market is expanding. After 1990s, the development of photovoltaic power generation is increasing rapidly. Until 2006, over 10 megawatt photovoltaic power generation systems and 6 megawatt networking photovoltaic power plant were built all over the world. The United States was the first country who made the development plan for photovoltaic power plant. They started "A Million Solar Roofs" plan [3] in 1997. Japan started "New Sunshine" plan [4] in 1993 and Japanese PV module production accounted for 50% of the world until 2003. There are 4 of world's top 10 PV companies in Japan. German provided the price of photovoltaic electricity in new renewable energy law, which greatly promoted the development of photovoltaic market and industry. Because of this, Germany become one of the fastest-growing country in photovoltaic. In addition, Switzerland, France, Italy, Spain, Finland and other countries have also made the plan for developing photovoltaic and invested heavily in technology development.

Comparing with other kinds of renewable energy, the advantages are concluded as safer and more convenient. It's evidenced by the statistics in the worldwide markets, which show the stable increasing ratio of solar energy in the total energy consumption will gradually increase to dominant ratio.

The top-most solar PV capacity countries such as Germany, Italy, USA, China, Japan, Spain,

France, Belgium, Australia and Czech republic had added new installed PV capacities by 7.6 GW, 3.6GW, 3.3GW, 3.5GW, 1.7GW, 0.2GW, 1.1GW, 0.6GW, 1GW and 0.1GW, respectively (shown in Figure 1, the last six years installed capacities) [5]. During the period of 2012, Germany has the most solar PV capacity with 28TWh electricity production, 45% more than 2011. Italy follows with the total capacity installation of 16.4 GW, but lower than the additions in 2011.

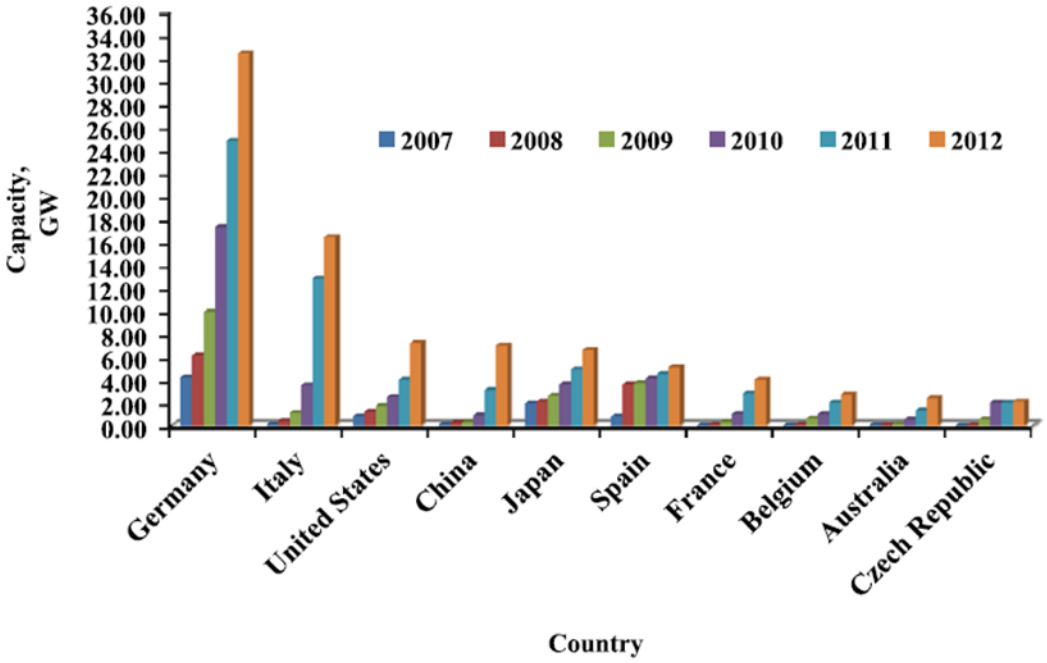

Figure 1 Solar PV cumulative installed capacity of the top ten countries in the past six years [5].

Figure 2 shows the top 10 solar PV companies ranking in 2012. There are 7 companies from Asia (6 companies from China and one company from Japan) among the top 10 ranking. Yingli won the first position with 2300 MW installation and then followed by First Solar (USA) and Trina Solar (USA) with 1800 MW and 1600 MW, respectively.

Sl. no.	Top ten solar module manufacturer's Name	Country	Installed in 2012 (MW)
1	Yingli	China	2300
2	First Solar	US	1800
3	Trina Solar	China	1600
4	Canadian Solar	China	1550
5	Suntech	China	1500
6	Sharp Solar	Japan	1050
7	Jhinko Solar	China	900
8	Sunpower	US	850
9	REC Group	Norway	750
10	Hanwha SolarOne	China	750

Figure 2 Top ten solar manufacturer suppliers in the world by the end of 2012 [5].

2 Hot zone development

Most of single crystals provided for semiconductor devices are produced by Czochralski (CZ) process. In CZ process, the temperature variation in crystal causes the thermal stress and results in the dislocation generation, while the shape of melt/crystal has effects on the the perfection of crystal and radial dopant distribution. Thus the heat transfer mechanism during the CZ process and shape of melt/crystal interface are two important factors.

Many hot zones have been designed by improving the ingot quality of Czochralski silicon. Recently, more and more people put their focus on cost reduction by increasing the efficiency of hot zone. Better designs make a significant decrease on consumables like graphite parts in furnace. In 1999, Siemens Solar Industries (SSI) and Northwest Energy Efficiency Alliance (NEEA) [8] had made a power-reduction project, which shown that 40% of power can be saved. Additionally, radiation shield is another invention to reduce the consumption. Shield is used for redirecting the argon flow and insulating the heat. Sinno's team had reported a molybdenum radiation shield on power reduction [14]. They delineated that the shape of the interface between the melt and solid could be kept in a tolerated level under the effect of the incorporated shield. At the same time, the pulling rate is increased to reduce the consumption of energy.

However, the pulling rate is also an important factor released to the production. In other words, increase the pulling rate can shorten the growth cycle.

In this thesis, an active cooling device was installed on the radiation shield will be discussed. This device is aimed to increase the temperature gradient near melt/crystal interface. Conclusions and discussions are given in Chapter 4.

3 Numerical modeling of Czochralski process

Due to the high cost and risk of crystal growth experiments, numerical simulation of CZ process becomes highly used as an effective tool to improve the structure of furnace and analysis the mechanism during the process. Especially the hot zone study, which has a great impact in defect evolution. X. Geng, X.B. Wu and Z.Y. Guo [16] simulated the combined flow in CZ crystal growth. V.V. Kalaev, I.Yu. Evstratov and Yu.N. Makarov [17] analyzed the role of gas flow to the heat transport, interface between melt and crystal, surface temperature and melt convection. Yutaka Shiraishi *et al.* [18]used global simulation to predict the shape of melt/crystal interface, and compare it with experimental data.

Chapter 2 Theory

This chapter will give the necessary theory on the crystal growth process including a general description of the process, heat transfer and fluid flow and dopant. The theoretical basis and assumption for the numerical modelling will be given as well.

1 The Czochralski process

Czochralski process was invented by J.Czochralski in 1917. In 1950, Teal and Little used CZ method in the growth of germanium and monocrystalline silicon. In 1958, Dash found a way to exclude the dislocation completely which made it possible to produce large size crystal [19]. The equipment and process of CZ crystal growth is relatively simple, easy to achieve automatic control, prepare large diameter crystal and control the concentration of impurities. It can produce low resistivity single crystal and it has high efficiency.

The stages of growth process is:

Melting

Melting step will take several hours, until the temperature in the hot zone reach to about 1500℃, and then retained there to make sure that all the feedstock in the filler are melt. When the whole filler is molten, the crucible will be uplifted to required starting position. Based on the previous growth experience, the temperature will be stabilized to close to a certain temperature. Under the monitor of pyrometer, the dip time of seed can be well controlled in a stable environment.

Necking

The lower part of seed will be melt at the certain temperature, then the seed is pulled up slowly. A meniscus will appear, then the new crystal will form. As introduced by Dash in the late 1950s, if the crystal is grown rapidly and thin enough, the dislocations will grow out from the sides of the neck eventually be frozen and excluded from the material [20]. So the neck is a rapid and short step to avoid dislocations.

Crown

The crown step will start when the correct temperature and proper length of the neck have been reached. The pull speed is lowered, the crucible rotation speed is changed as well as the melt level is adjusted to create a suitable conditions. This aims to obtain the proper diameter which too slow or too long will cause the structure loss. On the melt surface, with the increasing diameter, the freezing interface under the surface is increasing convex towards the melt as well, the shape will influence the chance of success of the crown and next steps significantly [20].

Body

The shape of the body is cylinder. There is an ephemeral period of time called shoulder. This

stops the crystal growth in diameter. When the shoulder is complete, the body will start. At this time, the temperature will go on doping a little slowly. The diameter of the body can be controlled smoothly by using the PID (proportional-integrating-derivative) control loop. The pulling speed is mainly adjusted by the heat power and temperature of hot zone. Gas flow, pressure, and crucible rotation rates are considered as well.

When the body part finished, typically at 10% of the melt will be remained in the crucible. A portion of this remaining is used to constitute tail.

Shut-off

The heater will be shut down after the tail step is completed. The crystal will be moved to receive chamber to cool down.

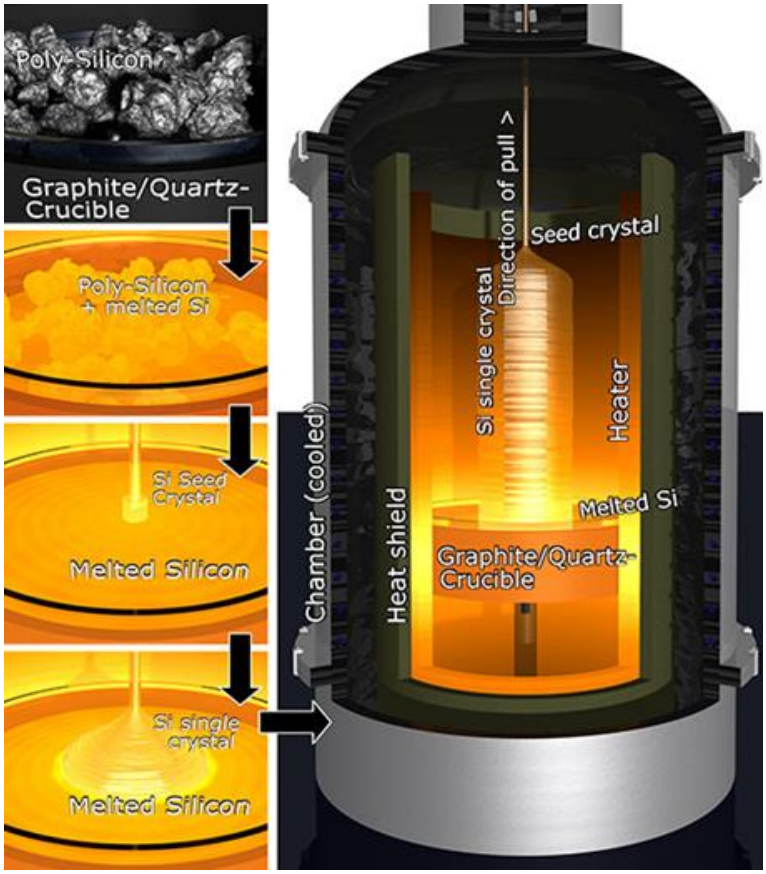

Figure 3 Czochralski process

2 Behaviors during the crystallization

1.1 Surface tension

A meniscus is formed in the growth interface during the crystal pulling due to the surface tension of the melt. The height of meniscus depends on the balance between the surface tension of the melt and its gravitational force.

1.2 Heat balance

When the silicon charge in the crucible was heated to its melting point to form a liquid completely, the melt growth starts. In a typical Cz puller, to create the temperature gradients on both vertical and radial direction in the melt, a thermal insulation will be applied on the outside of the heater and the bottom of the crucible. Therefore, the center of its free surface will get the lowest temperature. To start crystal growth, the melt temperature becomes lower and lower until the center of the melt surface has achieved the melting point. Then a single crystal seed will be dipped into the melt. After an equilibrium condition is set up, a further lowering will be done. The seed can be progressively pulled up from the melt once the freezing appears on it. The latent heat will occur during the freezing of molten silicon. The latent heat would block the further freezing of silicon if it is not removed timely. It will be transported into the crystal through conduction. After that the crystal transports the heat in to the surroundings via convection and radiation. Figure describes a typical heat flow mode during the crystal pulling. The heat goes into the system should equal to the heat that goes out in a steady state. If we use an equation, it should be like this:

$$Q_H + Q_L = Q_M + Q_C$$

Which Q_H means the heat from heater, Q_L means latent heat of solidification (heat input), and Q_M means the heat loss from the melt, Q_C means heat loss from crystal (heat output).

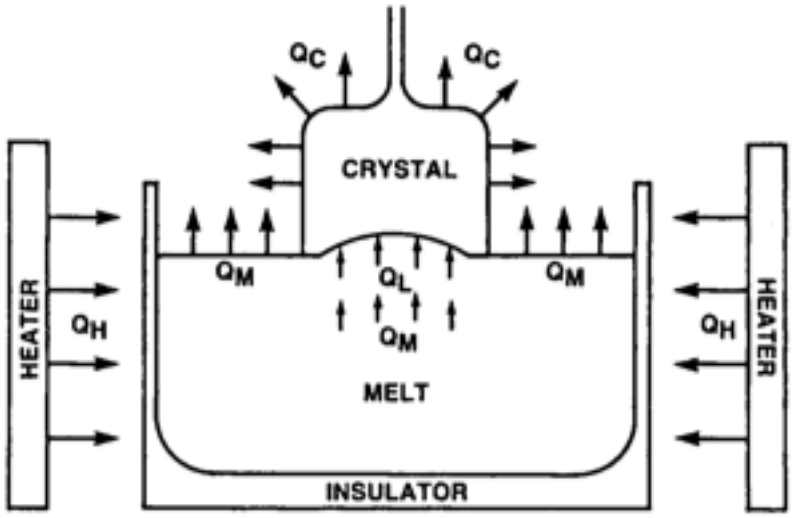

Figure 4 Heat balance during the Cz process

1.3 Convection

There are three essential principles during the crystal growth: a) the main heater should be installed around the crucible; b) the diameter of crucible should bigger than its height; c) the crystal and crucible should rotated along the central axis of symmetry. All of these principles are aim to remain the stable of the fluid.

There are mainly three kinds of convections in Cz process:

Natural convection

Since the heaters are installed in the surrounding and bottom of the crucible, the temperature of melt at the lateral and bottom are higher than the internal and top, respectively. Temperature changes the density of melt, which makes the melt flows from the bottom to the top.

The forced convection by the rotation of the crystal and crucible

In order to inhibit the natural convection, crystal and crucible needs to be rotated. Crucible rotation makes the thermal convective flow of the melt into spiral paths and improve the radial temperature gradient. Crystal rotation creates the supernumerary cell below the interface.

Surface tension convection

Surface tension convection are caused by the surface temperature difference. This convection plays a slight role during the Cz process.

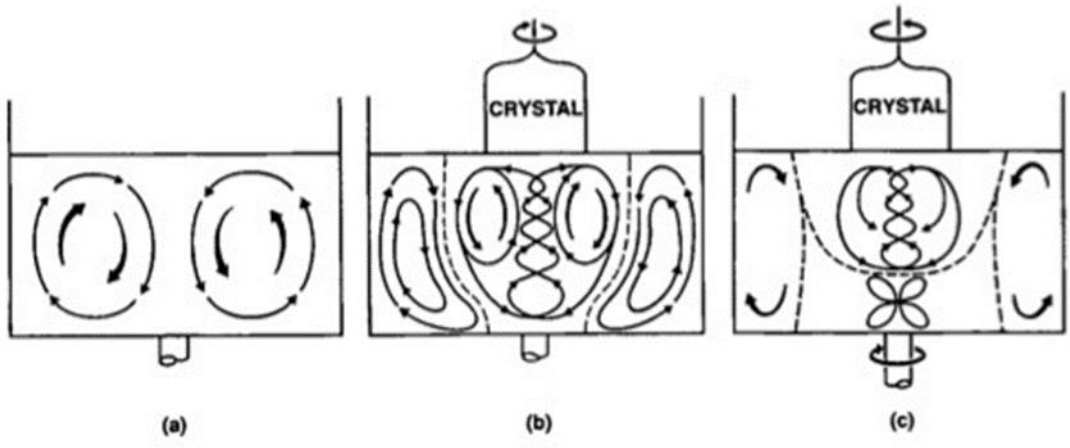

Figure 5 three kinds of convections

3 Numerical modeling of hot zone

We had simplified the following parts for convenience:

1. The thermal conductivity of seed is ignored;
2. The crown step is ignored;
3. Crystal is isotropic.

The mathematical model of hot zone is shown in Figure 6

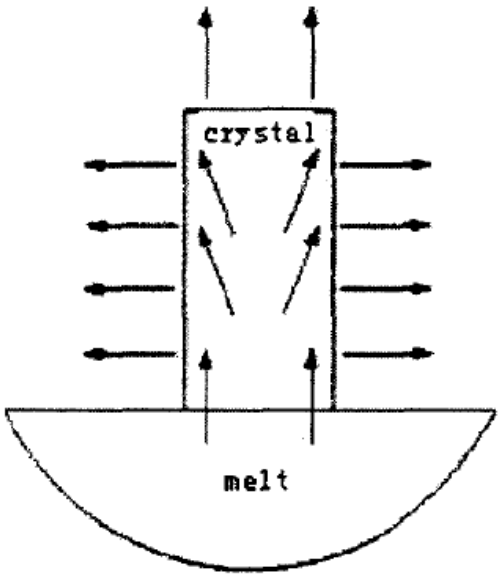

Figure 6 Heat map of crystal and melt.

The radius of crystal is a, length is l, density is ρ, specific heat capacity is c, thermal conductivity is k. The hot zone is supposed to be steady state. The differential equation is:

$$c\rho\frac{\partial T}{\partial t} = k\left(\frac{\partial^2 T}{\partial x^2} + \frac{\partial^2 T}{\partial y^2} + \frac{\partial^2 T}{\partial z^2}\right) \quad (1)$$

Using the cylindrical coordinate system, the coordinates of variables are represented by z, r and φ.

$$c\rho\frac{\partial T}{\partial t} = k\left(\frac{\partial^2 T}{\partial z^2} + \frac{\partial^2 T}{\partial \varphi^2} + \frac{\partial^2 T}{\partial r^2} + \frac{1}{r}\frac{\partial T}{\partial r}\right) \quad (2)$$

Suppose that the hot zone is cylindrical symmetry, and coaxial with the crystal. So T is the function of r and z. According to the equation, the heat conduction equation in steady state is:

$$\frac{\partial^2 T}{\partial r^2} + \frac{1}{r}\frac{\partial T}{\partial r} + \frac{\partial^2 T}{\partial r^2} = 0 \quad (3)$$

The boundary condition are:

At the solid-liquid interface, T equals to melting point T_m, so $T=T_m$, z=0.

At the top part, z=l, we assumed that the top part is a plane, the temperature of surrounding is T_0. The boundary condition at the top part is:

$$-\mathrm{k}\frac{\partial \mathrm{T}}{\partial \mathrm{z}} = \beta(T - T_0)^{1.25} + \mathrm{B}\sigma(T^4 - T_0^4) \quad z = l \tag{4}$$

which β is heat loss coefficient of convection, σ is Stefan-Boltzmann constant.

Also, the boundary condition at side face is:

$$-\mathrm{k}\frac{\partial \mathrm{T}}{\partial \mathrm{r}} = \beta(T - T_0)^{1.25} + \mathrm{B}\sigma(T^4 - T_0^4) \quad r = \mathrm{r}_a \tag{5}$$

Then the hot zone can be get by solving the heat conduction equation with three boundary conditions above. But the boundary conditions are usually nonlinear which make the second order partial differential equations hard to solve. Therefore we introduce the relative temperature function $\theta(r,z) = \mathrm{T}(r,z) - T_0$ to linearize the equation. Then the thermal conduction is transformed to:

$$\frac{\partial^2\theta}{\partial r^2} + \frac{1}{r}\frac{\partial\theta}{\partial r} + \frac{\partial^2\theta}{\partial r^2} = 0 \tag{6}$$

The boundary condition of it is:

$$\theta = \theta_m = T - T_0 \qquad z = 0 \tag{7}$$

After the function transformation, we get:

$$-k\frac{\partial \theta}{\partial \mathrm{z}} = \beta\theta^{1.25} + \mathrm{B}\sigma[(\theta + T_0)^4 - T_0^4] \tag{8}$$

It can be written as:

$$-\mathrm{k}\frac{\partial \theta}{\partial \mathrm{z}} = \beta\theta^{1.25} + 4B\sigma T_0^3\left[1 + \frac{3}{2}\left(\frac{\theta}{T_0}\right) + \left(\frac{\theta}{T_0}\right)^2 + \frac{1}{4}\left(\frac{\theta}{T_0}\right)^3\right]\cdot\theta \tag{9}$$

Make $\varepsilon_c = \beta\theta^{0.25}$, $\varepsilon_r = 4B\sigma T_0^3\left[1 + \frac{3}{2}\left(\frac{\theta}{T_0}\right) + \left(\frac{\theta}{T_0}\right)^2 + \frac{1}{4}\left(\frac{\theta}{T_0}\right)^3\right]$

We can get the linearized boundary condition:

$$k\frac{\partial \theta}{\partial \mathrm{r}} + \varepsilon\theta = 0 \qquad \mathrm{r} = r_a \tag{10}$$

$$\mathrm{k}\frac{\partial \theta}{\partial \mathrm{z}} + \varepsilon\theta = 0 \qquad \mathrm{z} = \mathrm{l} \tag{11}$$

which ε is heat exchange coefficient, it is the summary of convection exchange coefficient and radiation exchange coefficient. By using these boundary conditions, the equation can be solved.

$$\theta(r,z) \approx \theta_m \frac{(1 - hr^2/2a)}{\left(1 - \frac{1}{2}hr_a\right)} \exp\left\{-\left(\frac{2h}{r_a}\right)^{1/2} z\right\} \tag{12}$$

which $h = \frac{\varepsilon}{k}$ when $h > 0$, the heat in crystal is mostly dissipated to the environment through the crystal surface.

Temperature gradient analysis:

1. The radial temperature gradient can be known from equation (12):

$$\frac{\partial\theta}{\partial r} \approx -\theta_m \frac{2hr}{r_a\left(1 - \frac{1}{2}hr_a\right)} exp\left\{-\left(\frac{2h}{r_a}\right)^{1/2} z\right\} \tag{13}$$

when z is a constant,

$$\frac{\partial\theta}{\partial r} = \text{constant} \cdot exp\left\{-\left(\frac{2h}{r_a}\right)^{1/2} z\right\} \quad (14)$$

The radial temperature gradient will increase with increasing r.

2. The axial temperature gradient can be know from equation (14):

$$\frac{\partial\theta}{\partial z} \approx -\theta_m \left(\frac{2h}{r_a}\right) \frac{\left(1-hr^2/2a\right)}{\left(1-\frac{1}{2}hr_a\right)} \exp\left\{-\left(\frac{2h}{r_a}\right)^{1/2} z\right\} \quad (15)$$

when r is a constant,

$$\frac{\partial\theta}{\partial z} = constant \cdot (1 - hr^2/2a) \quad (16)$$

This means that the axial will decrease with increasing z.

The three equations (12) (13) (15) above are approximate expressions of temperature distribution in crystal, which was calculated by Bryce.

Disadvantages:

The calculation of this method is rather complex and its results are lack of universality. In addition, it is hard to get the solution when the boundary condition is irregular. Therefore the Finite Element Method is chosen as a mainly method in this thesis.

Numerical modeling of hot zone based on FEM

In some mathematic analysis example, the Finite Element Method (FEM) has widely used to finding approximate solutions in numerical technique as well as boundary value problems in partial differential equations. Deeply, the 'finite elements' means using whole problem domain into simpler parts subdivision. On the other hand, it could solve the problem by minimizing an associated error function by variational methods from the calculus of variations. FEM is similar to the concept of connecting multi tiny straight lines can approximate a large line or circle. Thus, finite elements could approximate a multi complex equation over a larger domain as well as include numerical methods to connection multi simple element equations over multi small sub-domains. Galerkin method is the mostly used variational method.

1.1 Galerkin method

Normally the problem is expressed as a differential equation:

$$\mathrm{A(u)} = \begin{Bmatrix} A_1(u) \\ A_2(u) \\ \vdots \end{Bmatrix} = 0 \quad (\ in\ \Omega\ ) \quad (17)$$

Boundary condition:

$$\mathrm{B(u)} = \begin{Bmatrix} B_1(u) \\ B_2(u) \\ \vdots \end{Bmatrix} = 0 \quad (\ in\ \Gamma) \quad (18)$$

Ω is the domain of the problem, Γ is the boundary of the problem, A and B are differential operators of the independent variables (spatial coordinates, time coordinates etc.).

Since all the differential equations hold in Ω domain, for arbitrary function,

$$\int_\Omega v^T A(u)d\Omega = \int_\Omega (v_1 A_1(u) + v_2 A_2(u) + \cdots)d\Omega = 0 \quad (19)$$

which $\upsilon = \begin{Bmatrix} v_1 \\ v_2 \\ \vdots \end{Bmatrix} = 0$ is the function vector, it is a group of arbitrary functions that equals the quantity of differential equations.

Similarly, since all the differential equations hold in boundary, for arbitrary function $\bar{\upsilon}$,

$$\int_\Gamma^{-T} B(u)d\Gamma = \int_\Gamma (\bar{v}_1 B_1(u) + \bar{v}_2 B_2(u) + \cdots)d\Gamma = 0 \quad (20)$$

Therefore, the integral form is:

$$\int_\Omega v^T A(u)d\Omega + \int_\Gamma^{-T} B(u)d\Gamma = 0 \quad (21)$$

Make an integration by parts, we can get another form,

$$\int_\Omega C^T D(u)d\Omega + \int_\Gamma E^T(\bar{v})F(u)d\Gamma = 0 \quad (22)$$

C, *D*, *E* and F are differential operators, for the problem, assume that the unknown function u can be expressed as an approximation function. Its general form is:

$$u \approx \tilde{u} = \sum_{i=1}^{n} N_i a_i = Na \quad (23)$$

a_i is undetermined parameters, N_i is called trial function, it is taken from a complete sequence of functions, it is linearly independent.

Obviously, if we choose limited numbers for n, the approximate solution cannot meet the requirements of the differential equation (17) and all the boundary condition equation (18). The residuals *R* and $\bar{R}$ will appear:

$$\begin{cases} A(u) - A(Na) = R \\ B(u) - B(Na) = \bar{R} \end{cases} \quad (24)$$

Use *n* numbers of specified functions to take place the arbitrary functions v and $\bar{v}$ in equation (20):

$$\int_\Omega W_j^T R d\Omega + \int \bar{W}_j^T \bar{R} d\Gamma = 0 \qquad (j = 1,2,\cdots,n) \quad (25)$$

The aim of this equation is to force the residuals equal to 0 in average.

$$\begin{cases} \int_\Omega W_1^T A(Na)d\Omega + \int_\Gamma \bar{W}_1^T B(Na)d\Gamma = 0 \\ \int_\Omega W_2^T A(Na)d\Omega + \int_\Gamma \bar{W}_2^T B(Na)d\Gamma = 0 \\ \int_\Omega W_n^T A(Na)d\Omega + \int_\Gamma \bar{W}_n^T B(Na)d\Gamma = 0 \end{cases} \quad (26)$$

If the number of differential equations $A(u) = 0$ is m_1, the number of boundary conditions $B(u) = 0$ is m_2, then the weight function $W_j(j = 1,2,\cdots,n)$ is a m_1 order function array, $\bar{W}_j(j = 1,2,\cdots,n)$ is a m_2 order function array. The more the *n* is, the more accuracy we can get. When n tends to infinity, approximate solutions will converge to the exact solution.

If we made:

$$W_j = N_j$$

On the boundary, we made:

$$\bar{W}_j = -W_j = -N_j$$

The approximate integral form can be write as:

$$\int_\Omega N_j^T A(\sum_{i=1}^n N_i a_i)d\Omega + \int_\Gamma N_j^T B(\sum_{i=1}^n N_i a_i)d\Gamma = 0 \quad (j = 1,2,\cdots,n) \tag{27}$$

1.2 Calculation of hot zone

1.2.1 Control equations and boundary conditions

The differential equations of two-dimensional steady-state hot zone is:

Control equation:

$$k\left(\frac{\partial^2 T}{\partial x^2} + \frac{\partial^2 T}{\partial y^2}\right) - \rho Q = 0 \tag{28}$$

Dirichlet boundary condition:

$$T = T_c \tag{29}$$

Neumann boundary condition:

$$-k\frac{\partial T}{\partial x}n_x - k\frac{\partial T}{\partial y}n_y = q \tag{30}$$

Cauchy boundary condition:

$$-k\frac{\partial T}{\partial x}n_x - k\frac{\partial T}{\partial y}n_y = h(T_a - T) \tag{31}$$

Which ρ is the density, c is the heat capacity, T is temperature *(T=T(x,y))*.

According the Dirichlet boundary condition, we assume an approximate function, the residuals will appear:

$$R_\Omega = k\left(\frac{\partial^2 \tilde{T}}{\partial x^2} + \frac{\partial^2 \tilde{T}}{\partial y^2}\right) + \rho Q \tag{32}$$

$$R_{\Gamma_2} = k\frac{\partial \tilde{T}}{\partial x}n_x - k\frac{\partial \tilde{T}}{\partial y}n_y - q \tag{33}$$

$$R_{\Gamma_3} = k\left(\frac{\partial \tilde{T}}{\partial x}n_x + \frac{\partial \tilde{T}}{\partial y}n_y\right) - h(T_a - \tilde{T}) \tag{34}$$

According to the Galerkin method, the domain and boundary must meet to the problem.

$$\iint_\Omega w_1 R_\Omega \, d\Omega + \int_{\Gamma_2} w_2 R_{\Gamma_2} \, d\Gamma + \int_{\Gamma_3} w_3 R_{\Gamma_3} \, d\Gamma = 0 \tag{35}$$

$$\iint_\Omega w_1\left[k\left(\frac{\partial^2 \tilde{T}}{\partial x^2} + \frac{\partial^2 \tilde{T}}{\partial y^2}\right) + \rho Q\right]d\Omega + \int_{\Gamma_2} w_2\left[k\frac{\partial \tilde{T}}{\partial x}n_x - k\frac{\partial \tilde{T}}{\partial y}n_y - q\right]d\Gamma + \int_{\Gamma_3} w_3\left[k\left(\frac{\partial \tilde{T}}{\partial x}n_x +\right.\right.$$

$$\frac{\partial \tilde{T}}{\partial y} n_y \Big) - h(T_a - \tilde{T}) \Big] d\Gamma = 0 \quad (36)$$

and

$$\iint_\Omega \; w_1 \left[k \left(\frac{\partial^2 \tilde{T}}{\partial x^2} + \frac{\partial^2 \tilde{T}}{\partial y^2} \right) + \rho Q \right] d\Omega = \iint_\Omega \; k w_1 \frac{\partial^2 \tilde{T}}{\partial x^2} d\Omega +$$

$$\iint_\Omega \; k w_1 \frac{\partial^2 \tilde{T}}{\partial y^2} d\Omega + \iint_\Omega \; w_1 \rho Q d\Omega \quad (37)$$

Make a partial integration for the first and second terms in above equation and according to Green's theorem, we can get:

$$\iint_\Omega \; k w_1 \frac{\partial^2 \tilde{T}}{\partial x^2} d\Omega = \oint k w_1 \frac{\partial \tilde{T}}{\partial x} d\Gamma - \iint k \frac{\partial w_1}{\partial x} \frac{\partial \tilde{T}}{\partial x} d\Omega \quad (38)$$

$$\iint_\Omega \; k w_1 \frac{\partial^2 \tilde{T}}{\partial y^2} d\Omega = \oint k w_1 \frac{\partial \tilde{T}}{\partial y} d\Gamma - \iint k \frac{\partial w_1}{\partial y} \frac{\partial \tilde{T}}{\partial y} d\Omega \quad (39)$$

Set them in to the equation (37):

$$- \iint_\Omega \; k \left(\frac{\partial w_1}{\partial x} \frac{\partial \tilde{T}}{\partial x} + \frac{\partial w_1}{\partial y} \frac{\partial \tilde{T}}{\partial y} \right) d\Omega$$

$$+ \iint_\Omega \; \rho Q w_1 d\Omega + \oint_\Gamma \; k w_1 \left(\frac{\partial \tilde{T}}{\partial x} n_x + \frac{\partial \tilde{T}}{\partial y} n_y \right) d\Gamma + \int_{\Gamma_2} w_2 \left[k \left(\frac{\partial \tilde{T}}{\partial x} n_x + \frac{\partial \tilde{T}}{\partial y} n_y \right) - q \right] d\Gamma +$$

$$\int_{\Gamma_3} w_3 \left[k \left(\frac{\partial \tilde{T}}{\partial x} n_x + \frac{\partial \tilde{T}}{\partial y} n_y \right) - h(T_a - \tilde{T}) \right] d\Gamma = 0 \quad (40)$$

1.2.2 Elements division and hot zone discretization

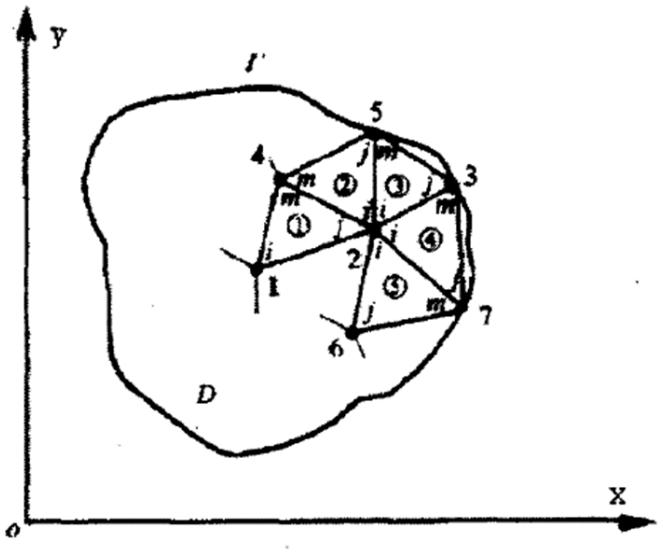

Figure 7 Schematic diagram of region is divided into the triangular element.

Divided the domain into finite numbers of triangular elements, for each triangular element, it satisfied:

$$\iint_{\Omega^e} w_1 R_\Omega \, d\Omega + \int_{\Gamma_2{}^e} w_2 R_{\Gamma_2} \, d\Gamma + \int_{\Gamma_3{}^e} w_3 R_{\Gamma_3} \, d\Gamma = 0 \tag{41}$$

$$- \iint_{\Omega^e} k \left(\frac{\partial w_1}{\partial x} \frac{\partial \tilde{T}}{\partial x} + \frac{\partial w_1}{\partial y} \frac{\partial \tilde{T}}{\partial y} \right) d\Omega + \iint_{\Omega^e} \rho Q w_1 d\Omega + \oint_{\Gamma^e} k w_1 \left(\frac{\partial \tilde{T}}{\partial x} n_x + \frac{\partial \tilde{T}}{\partial y} n_y \right) d\Gamma +$$

$$\int_{\Gamma_2{}^e} w_2 \left[k \left(\frac{\partial \tilde{T}}{\partial x} n_x + \frac{\partial \tilde{T}}{\partial y} n_y \right) - q \right] d\Gamma + \int_{\Gamma_3{}^e} w_3 \left[k \left(\frac{\partial \tilde{T}}{\partial x} n_x + \frac{\partial \tilde{T}}{\partial y} n_y \right) - h(T_a - \tilde{T}) \right] d\Gamma = 0$$

If the elements are tiny enough, then every element can be considered as linear distribution. Assume that the temperature $\tilde{T}$ is linear function and its coordinate is x, y. Set the coordinate of nodes i, j, k for one element as (x_l, y_l), l= i, j, k, the temperature of node are T_i, T_j, T_k. The temperature in element can be expressed as:

$$T = a_1 + a_2 x + a_3 y \tag{42}$$

Which a_1, a_2, a_3 are undetermined coefficients, it can be solved by the temperature of nodes.

$$\begin{bmatrix} T_i \\ T_j \\ T_k \end{bmatrix} = \begin{bmatrix} 1 & x_i & y_i \\ 1 & x_j & y_j \\ 1 & x_k & y_k \end{bmatrix} \begin{bmatrix} a_1 \\ a_2 \\ a_3 \end{bmatrix} \tag{43}$$

$$\begin{bmatrix} a_1 \\ a_2 \\ a_3 \end{bmatrix} = \frac{1}{2\Delta} \begin{bmatrix} a_i & a_j & a_k \\ b_i & b_j & b_k \\ c_i & c_j & c_k \end{bmatrix} \begin{bmatrix} T_i \\ T_j \\ T_k \end{bmatrix} \tag{44}$$

$$\begin{array}{lll} a_i = x_j x_k - x_k y_j & b_i = y_j - y_k & c_i = x_k - x_j \\ a_j = x_k x_i - x_i y_k & b_j = y_k - y_i & c_j = x_i - x_k \\ a_k = x_i x_j - x_j y_i & b_k = y_i - y_j & c_k = x_j - x_i \end{array} \tag{45}$$

Δ is the area of the triangle.

$$T = \frac{1}{2\Delta} \left[(a_i + b_i + c_i) T_i + (a_j + b_j + c_j) T_j + (a_k + b_k + c_k) T_k \right] \tag{46}$$

Transform it in to matrix form:

$$[T]^e = [N]\{T\}^e \tag{47}$$

which

$$[N] = \left[N_i, N_j, N_k \right]$$

$$N_i = \frac{a_i + b_i + c_i}{2\Delta}$$

$$N_j = \frac{a_j + b_j + c_j}{2\Delta}$$

$$N_k = \frac{a_k + b_k + c_k}{2\Delta}$$

$$\{T\}^e = \begin{bmatrix} T_i \\ T_j \\ T_k \end{bmatrix}$$

In this way, temperature in element can be approximate expressed by three nodes temperature.

According to Galerkin method:

$$w_l = \frac{\partial \tilde{T}}{\partial T_l} N_l (l = i, j, k) \tag{48}$$

$$-\iint_{\Omega^e} k \left(\frac{\partial N_l}{\partial x} \frac{\partial [N]}{\partial x} + \frac{\partial N_l}{\partial y} \frac{\partial [N]}{\partial y} \right) \{T\}^e d\Omega + \iint_{\Omega^e} \rho Q N_l d\Omega + \iint_{\Gamma_2^e} N_l q d\Gamma + \int_{\Gamma_3^e} N_l h T_a d\Gamma -$$

$$\int_{\Gamma_3^e} N_l h [N] \{T\}^e d\Gamma = 0 \tag{49}$$

Transform it into matrix form:

$$\iint_{\Omega^e} k \left(\left(\frac{\partial [N]}{\partial x} \right)^T \frac{\partial [N]}{\partial x} + \left(\frac{\partial [N]}{\partial y} \right)^T \frac{\partial [N]}{\partial y} \right) \{T\}^e d\Omega - \iint_{\Omega^e} \rho Q N_l d\Omega - \iint_{\Gamma_2^e} [N]^T q d\Gamma -$$

$$\int_{\Gamma_3^e} [N]^T h T_a d\Gamma - \int_{\Gamma_3^e} [N]^T h [N] \{T\}^e d\Gamma = 0 \tag{50}$$

The equations above are used to determine the temperature of three nodes for one element. They can be written as the general finite element format:

$$[k]^e \{T\}^e = [p]^e \tag{51}$$

which $[k]^e$ is heat transfer matrix, $[p]^e$ is unit temperature loading matrix caused by heat exchange.

1.2.3 Synthesis

After finishing the calculation of per element, we need to sum all the element calculation results. The main purpose for this step is construct the total heat transfer matrix [K]. Specifically, calculate each heat transfer matrix firstly, and then set the results into the corresponding positions in total heat transfer matrix. At last, we can get total heat transfer matrix by summing up the results in same position.

$$[K]\{T\} = [P] \tag{52}$$

$$\begin{bmatrix} k_{11} & k_{12} & \cdots & k_{1n} \\ k_{21} & k_{22} & \cdots & k_{2n} \\ \vdots & \vdots & \cdots & \vdots \\ k_{n1} & k_{n2} & \cdots & k_{nn} \end{bmatrix} \begin{bmatrix} T_1 \\ T_2 \\ \vdots \\ T_n \end{bmatrix} = \begin{bmatrix} P_1 \\ P_2 \\ \vdots \\ P_n \end{bmatrix} \tag{53}$$

1.2.4 Iterative solution

For the two-dimensional axisymmetric heat transfer problem, the finite element equation is nonlinear, Newton-Raphson method is a better way to solve the problem.

The equation (52) can be converted to:

$$[P^{nr}] = [p^a] \tag{54}$$

which $[P^{nr}]$ is internal node heat flux vector, $[p^a]$ is the node heat flux vector caused by load.

Initially, internal node heat flux and node load are not equal, the difference of these two vectors is called 'residual'. It can be represented by:

$$\{\phi\} = [p^a] - [P^{nr}] \tag{55}$$

By using Newton-Raphson method, $\{\phi\}$ can be decreased to zero, this process is called convergence. Specific steps are as follows:

1. Solve the incremental form of the equations.

$$\begin{cases} [K_i]\{\Delta T_i\} = [p^a] - [P^{nr}] \\ \{T_{i+1}\} = +\{\Delta T_i\} \end{cases} \tag{56}$$

2. Update the node temperature.
3. Calculate the internal node heat flux rate by element heat flux.
4. Calculate the convergence results and compare with convergence criteria.
   If the result is smaller, no longer iterate.
   If the result is larger or equal, [Ki] is updated and repeat the process.

1.2.5 Summary

The mainly numerical calculation can be show as:

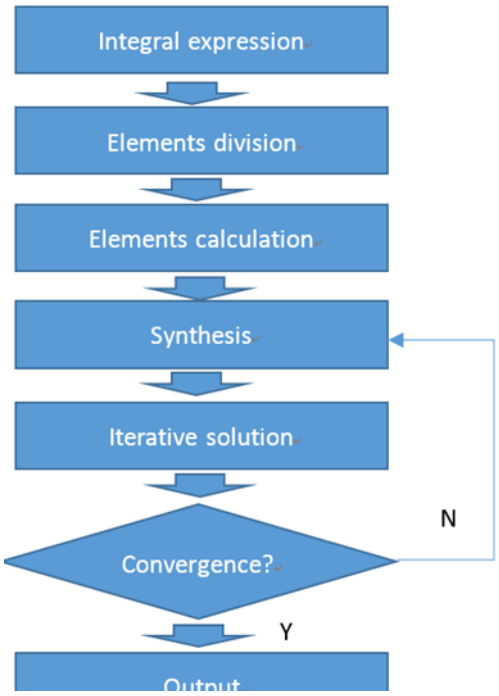

Figure 8 Flow chart of numerical calculation

4 CGSim (Crystal Growth Simulator)

The CGSim is a specialized software for the simulation of crystal growth processes. The software provides information about the most important physical processes involved into crystal growth and affecting crystal quality. The mainly used part of CGSim in this thesis is CGSim-2D simulation [9]-[14].

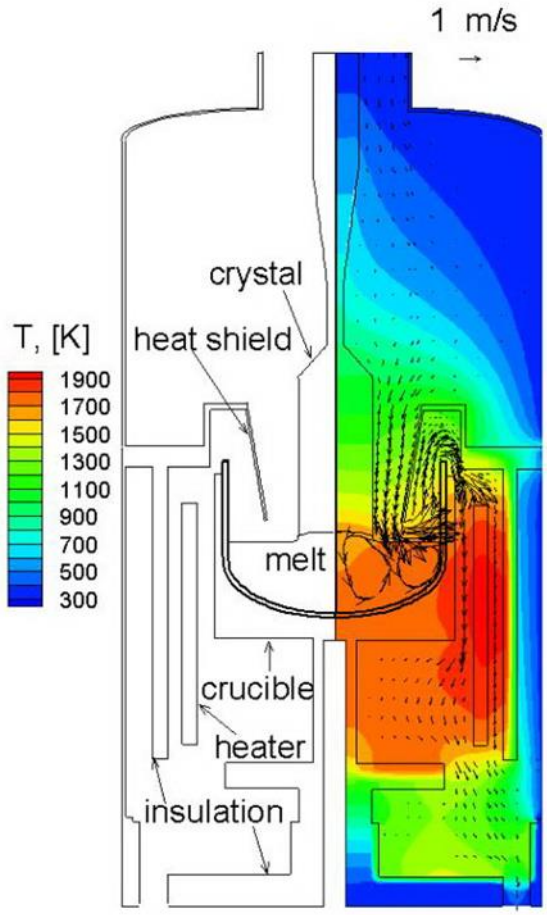

Figure 9 CGSim simulator.

Chapter 3 Simulation settings

The aim of the work is to simulate the effect of the cooling jacket to the hot-zone during the Czochralski growth. CGSim is a kind of crystal growth simulation software which can forecast the global hot-zone in the furnace, gas flow, the shape of the melt/crystal interface, the shape of melt free surface, the crystallization rate and the power consumption in crystal. A large number of experiments have verified the simulation results.

1 Basic model

2D axisymmetric model is established due to the real Cz furnace from SINTEF. Figure 10 shows the structure of the furnace, the computation grid cells are show in it. The grids in zones of the melt/crystal interface are refined. The height of crystal is 1500 mm, the diameter of the crystal is 200mm, the weight of feedstock is, the rate of crystal rotation is 10 rpm, the rate of crucible rotation is -10 rpm, the basic pull rate is 1.4 mm/min and the furnace pressure is 2000 Pa. The parameters of the materials are shown in Figure 11.

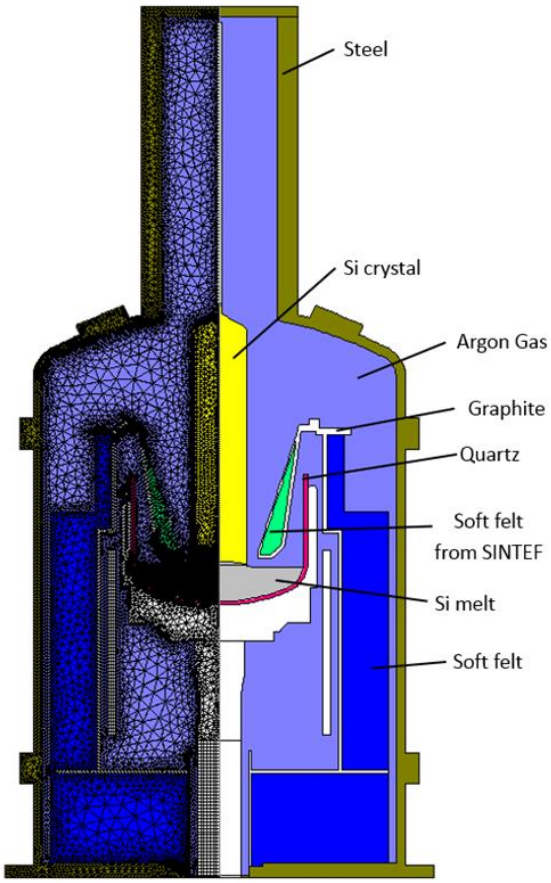

Figure 10 2D axisymmetric model of furnace.

Materials	Heat capacity (J/kg)	Heat conductivity (W/m)	Emissivity
Si(crystal)	1000	$98.89-9.42e^{-2}T+2.89e^{-5}T^2$	$0.9016-2.6208e^{-4}T$
Si(melt)	915	66	0.318
Graphite-p	500	$105(T/300)^{\wedge}(-0.3)\exp(-3.5(T-300)1e^{-4})$	0.8
Graphite felt	$0.634T+516$	$0.1773\exp[0.7\times10^{-3}(T-273)]$	0.9
Ar	520.8	$0.01+2.5e^{-5}T$	–
Quartz crucible	900	4	0.85
Non-corrosive steel	437.5	15	0.45

Figure 11Physical parameters of materials

2 Installation of the cooling jacket proposed attempted

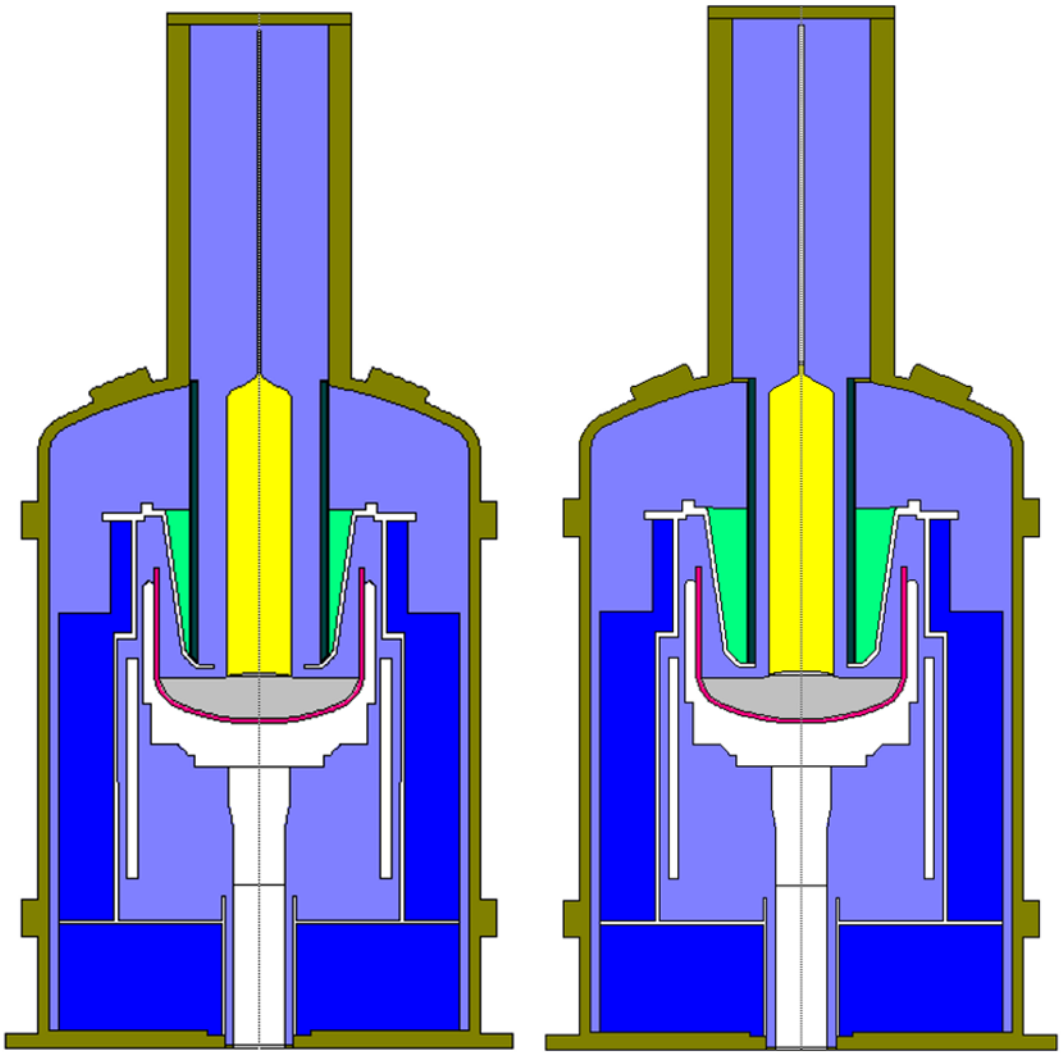

Figure 12 two different cooling jacket installation, case 2 (left) and case 3 (right).

Figure 12 shows two different ways of the cooling jacket installation. The inner part of original shield was removed and a steel tube is installed on the shield, the cylinder wall is hollow and a curve steel pipe is twined in it. The inlet and the outlet of pipe are all connected with the wall of the furnace. The space between the tube and shield is full filled up with the soft felt. By passing the water into the pipe, the heat can be removed from the cooling jacket. The temperature near the crystal/melt surface will decrease, which can increase the crystallization rate. Set the original model as case 1, two models with cooling jacket as case 2 and case 3, respectively.

For detailed study, there are 5 different crystal positions set up in this thesis, cp 100, cp 400, cp 750, cp 1100, cp 1400. Figure 13 shows all the crystal positions in the study (Case 1 as an example).

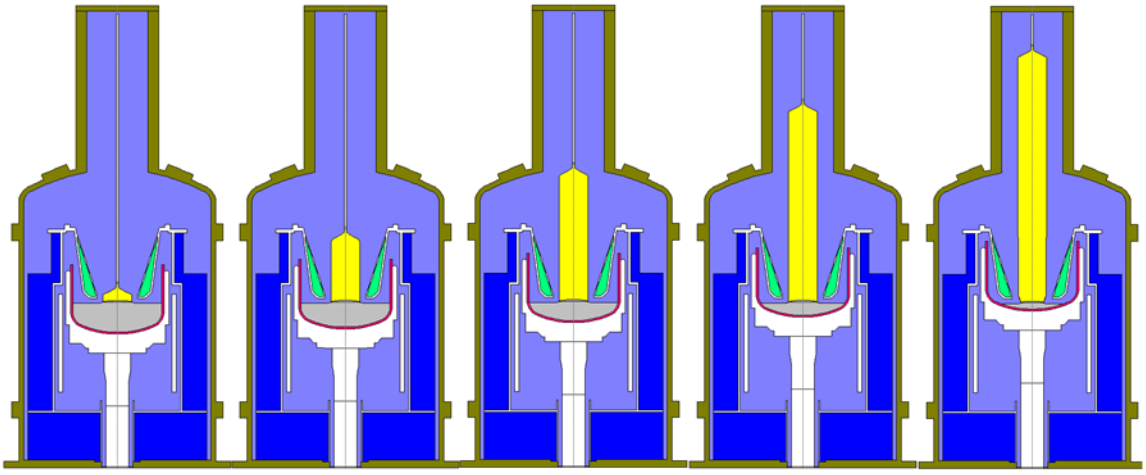

Figure 13 5 crystal positions during Cz process

Chapter 4 Results and discussion

1 Hot zone after installing the cooling jacket

As shown in Figure 14 (use the crystal position 750 as an example), after installing the cooling jacket, the isotherm in Case 2 and Case 3 are flatter than Case 1, which is beneficial to decrease the thermal stress in crystal [14]. It is good for obtaining a uniform solute segregation.

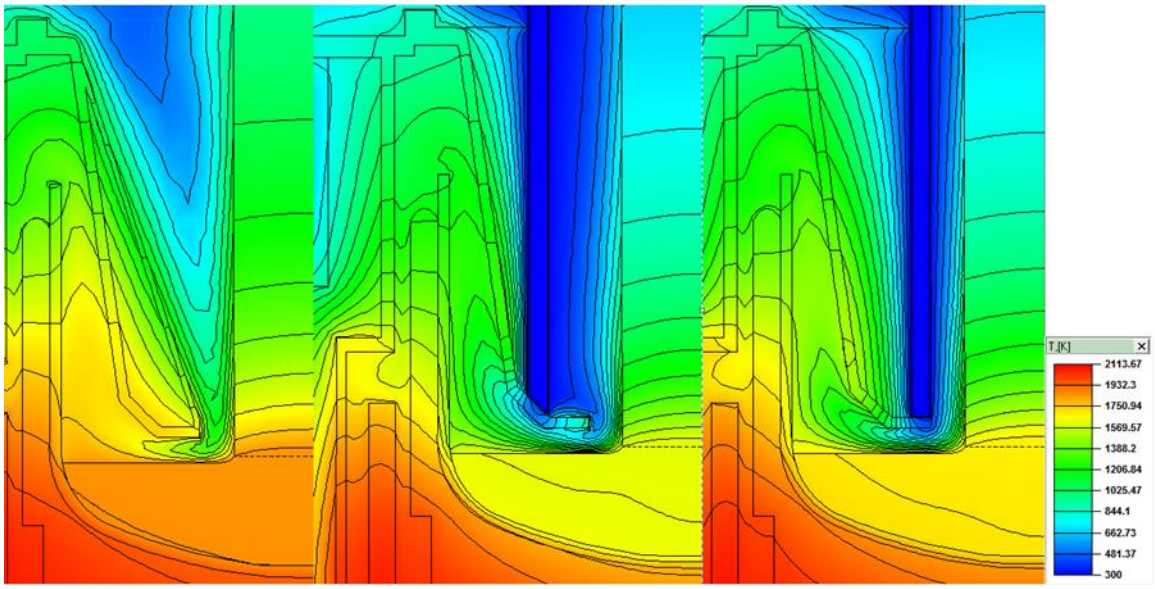

Figure 14 Comparison of hot zones.

2 Crystallization rate after installing the cooling jacket

The crystallization rate is proportional to the heat flux difference between crystal and melt in melt/crystal interface.

$$V_{crys} = (K_s G_s - K_l G_l)\rho_l L$$

Which K_s and K_l are the crystal conductivity and melt conductivity, respectively, G_s and G_l are the temperature gradients in crystal and temperature gradients in melt, respectively, L is the latent heat.

From the equation we know that there are two methods to improve the crystallization rate: the first is to increase the crystal temperature gradient, the second is to decrease the melt temperature gradient.

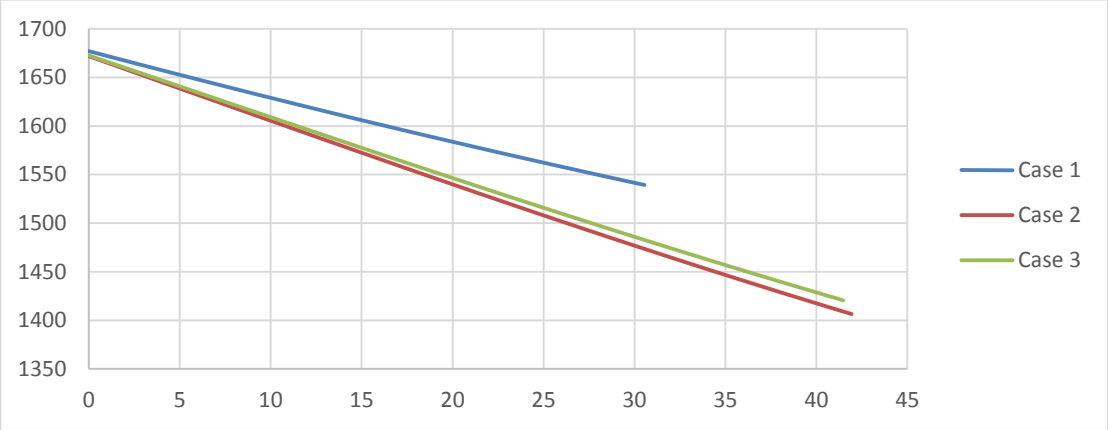

Figure 15 Temperature distributions in three cases along the axis of the crystal.

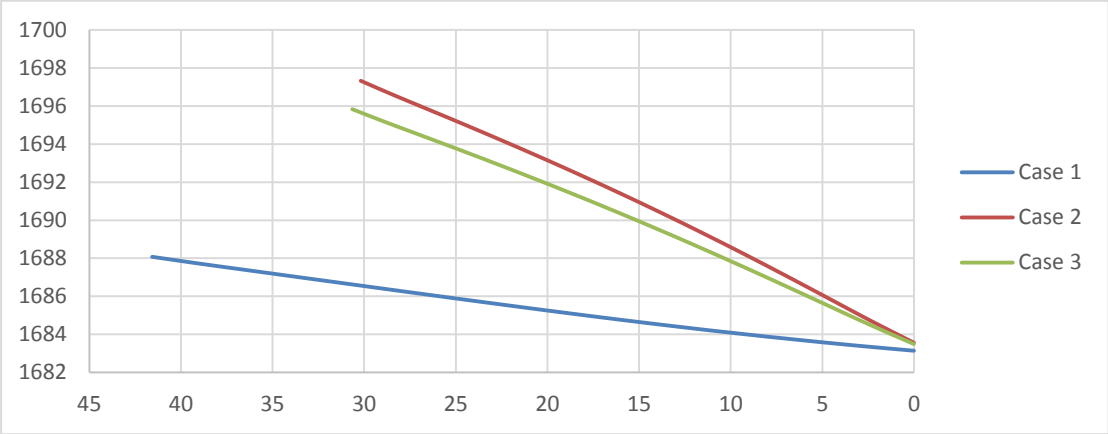

Figure 16 Temperature distributions in three cases along the axis of the melt.

Figure 15 shows the temperature distributions in three cases along the axis of the crystal, the X axis and Y axis are the distance from the interface along the axis of crystal and temperature, respectively. We can see that the temperature gradient in crystal increases (steeper slope). On the other hand, Figure 16 shows the temperature distributions in three cases along the axis of the melt, it is obviously that the temperature gradient in melt increases as well. But the slope is smaller than the temperature in crystal. According to the equation, the crystallization rate is increased after installing the cooling jacket. Correspondingly, the pull rate can be improved.

3 Melt temperature distribution after installing the cooling jacket

In Cz silicon process, there are mainly two factors have impacts on the quality of single crystal. One is the melt free surface temperature, the supercooling may be caused if the temperature of

melt free surface reduced in excess, resulting in dendritic or cellular crystal growth. The other is melt/crucible interface temperature, the crucible inside wall will have a reaction with silicon melt if the melt/crucible interface is overheated. This will cause excessive oxygen impurities. Figure 18 to Figure 21 show the melt surface temperature of different crystal positions in different cases. It is obviously that the average temperature of the melt free surface is around 10 ºC higher in case 2 and 3, thus to avoid supercooling. On the other hand, Figure 23 to Figure 26 display the temperature distribution of melt/crucible interface. In case 2 and 3, there are about 20 ºC higher than case 1. This region may cause oxygen generation. This is a disadvantage for the cases with cooling jacket. The reason for this situation may be that there is no insulation between the bottom of cooling jacket and shield and too much heat is absorbed from the melt surface. This disadvantage is improved in the next case.

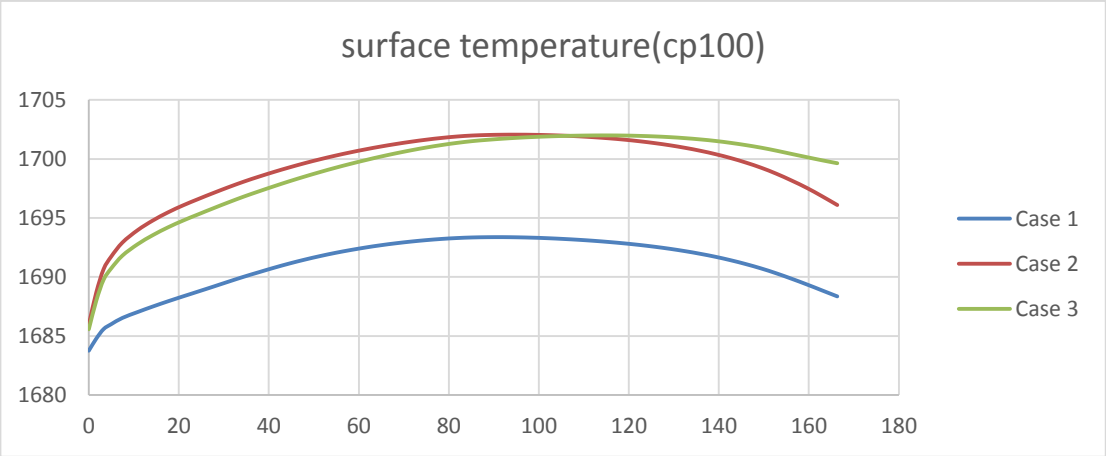

Figure 18 melt free surface temperature for three cases at crystal position 100.

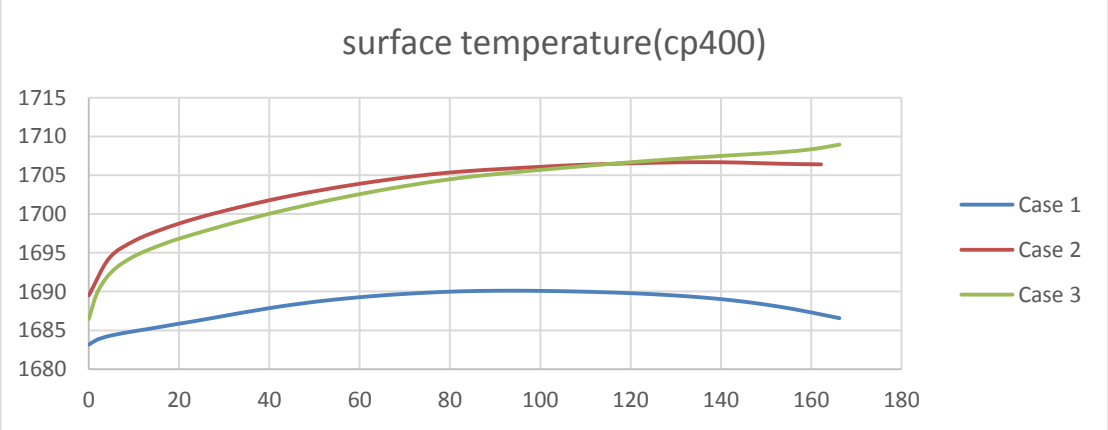

Figure 17 melt free surface temperature for three cases at crystal position 400.

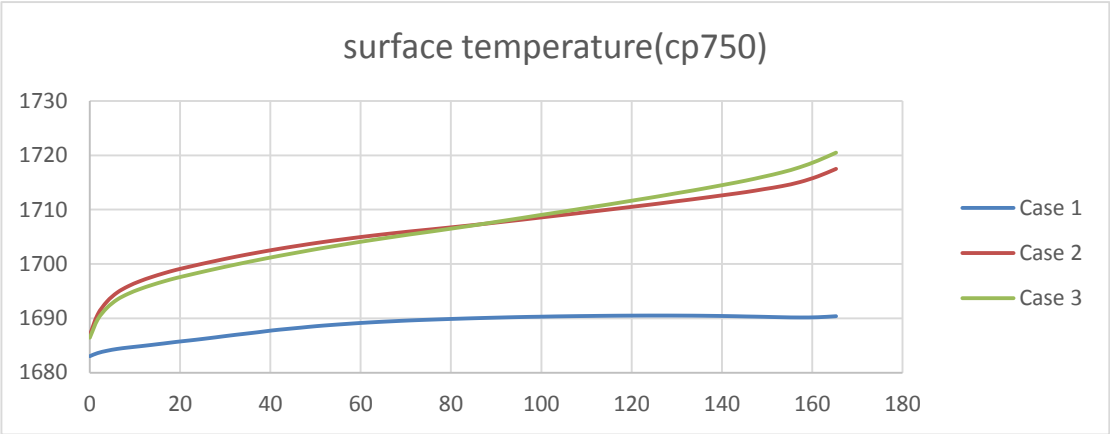

Figure 19 melt free surface temperature for three cases at crystal position 750.

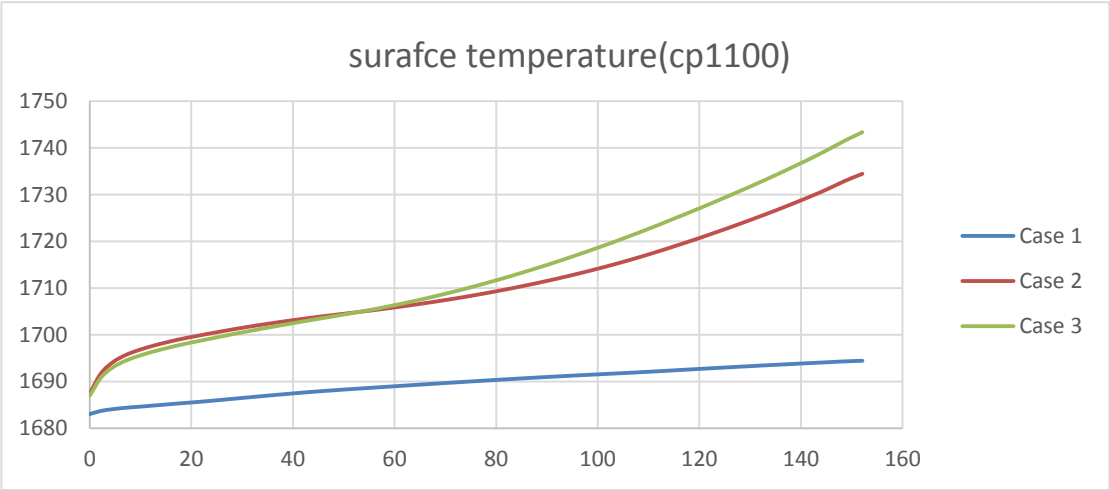

Figure 20 melt free surface temperature for three cases at crystal position 1100.

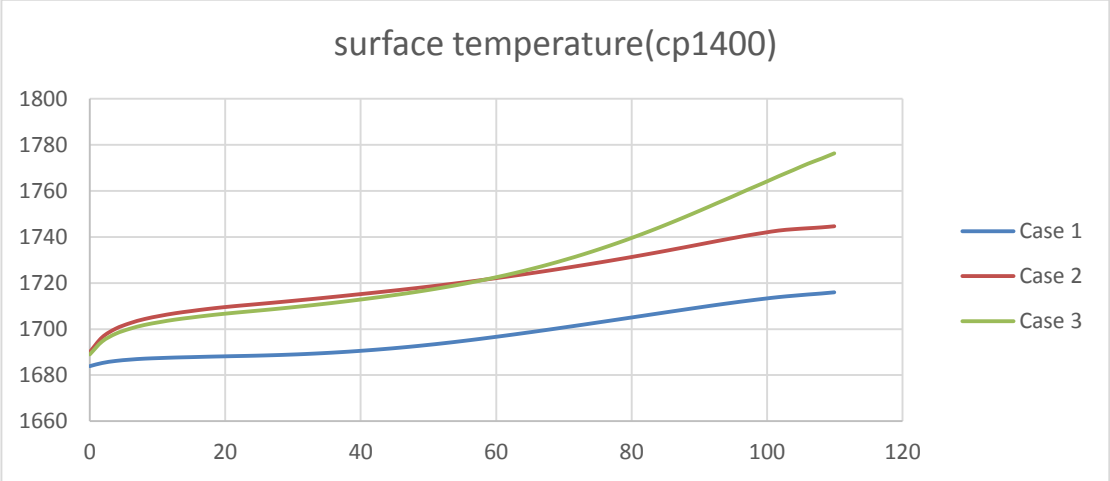

Figure 21 melt free surface temperature for three cases at crystal position 1400.

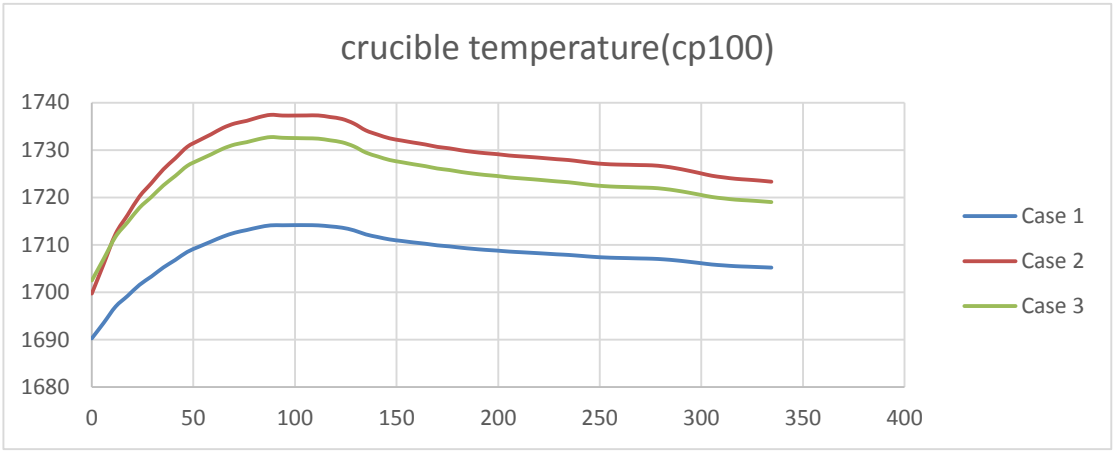

Figure 22 melt/crucible interface temperature for three cases at crystal position 100.

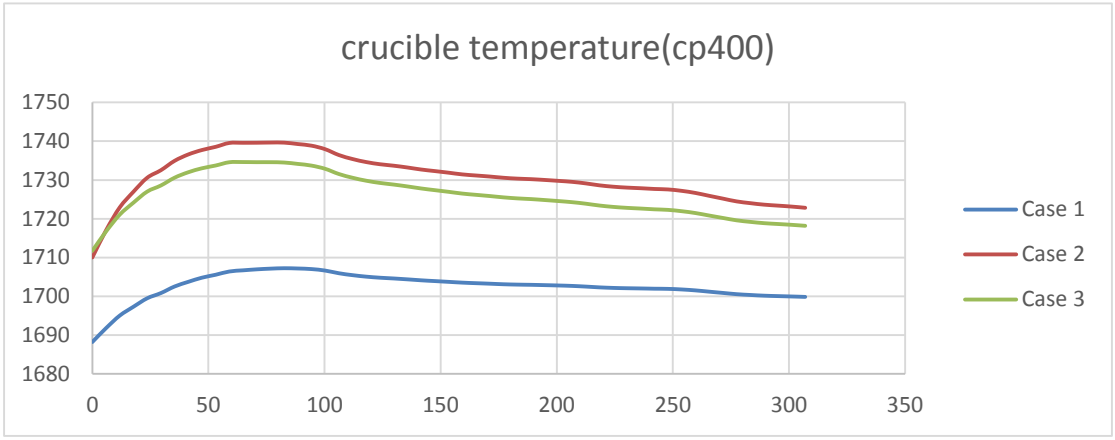

Figure 23 melt/crucible interface temperature for three cases at crystal position 400.

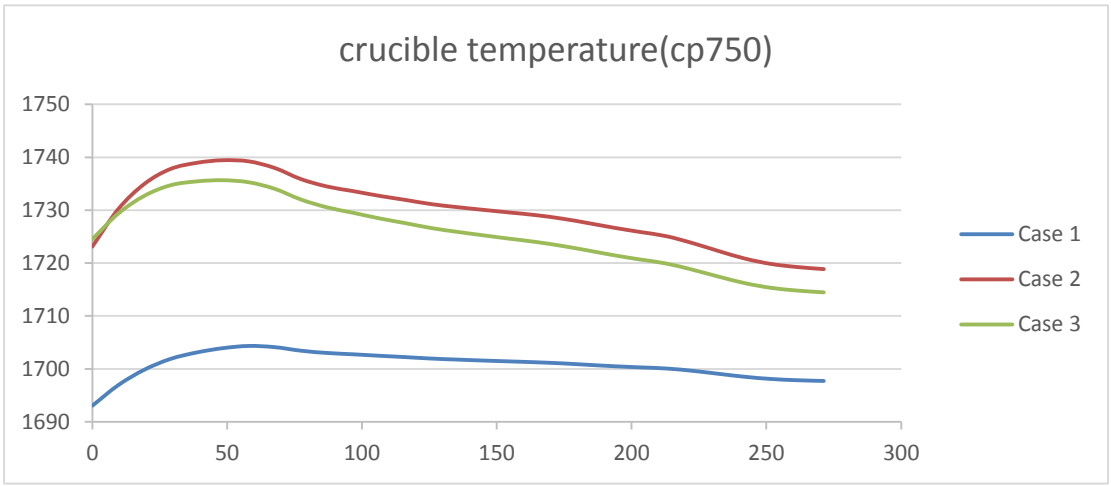

Figure 24 melt/crucible interface temperature for three cases at crystal position 750.

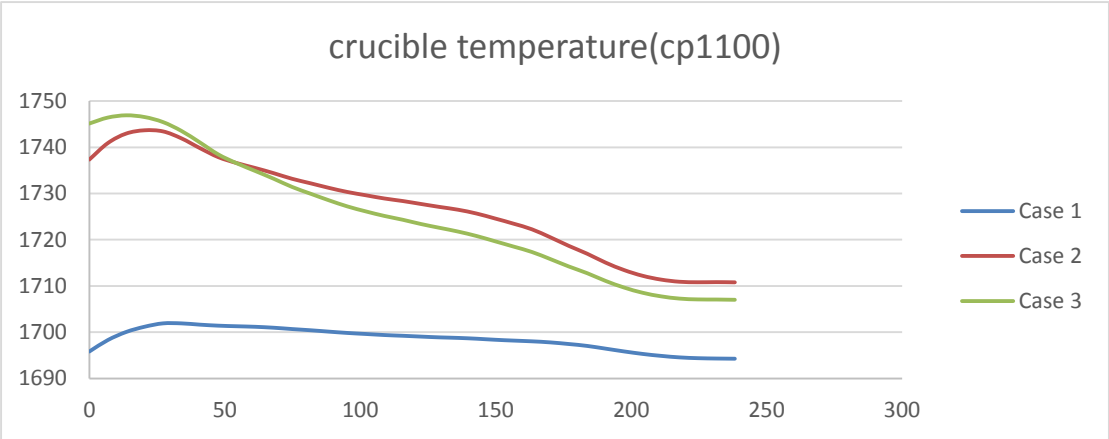

Figure 25 melt/crucible interface temperature for three cases at crystal position 1100.

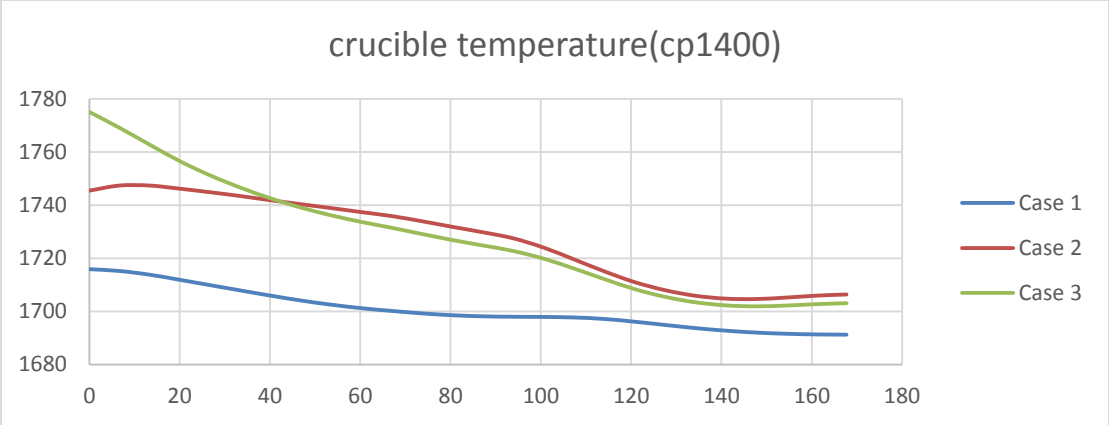

Figure 26 melt/crucible interface temperature for three cases at crystal position 1400.

4 Solid-liquid interface deflection after installing the cooling jacket

During the Cz process, if we neglect the supercooling of silicon melt, the temperature in melt/crystal interface is equivalent to the silicon melting point (1693ºC). There are four types of the interface deflection: concave up, concave down, flat and mixed with former three. Normally, at crown step, the interface is concave, then it becomes flat during body step, later, it changes to concave up. Regardless of which step, for guaranteeing the monocrystalline silicon growth quality, keeping the interface at a quasi-flat should be maintained.

The melt/crystal interface deflection can be influenced by many factors, such as the pull rate, the temperature gradients near interface, heat transfer on interface, melt convection, etc. By adjusting the parameters above, the deflection of melt/crystal interface can be well controlled.

The above parameters can be adjusted to change the deflection of solid-liquid interface. To obtain the satisfied quality of crystal, the height of melt/crystal interface is required to be

controlled practically in quasi-flat (less than 8mm) without a strong deviation up or down. Figure 27 to Figure 31 show the deflection of the melt/crystal interface of different crystal position for three cases at pulling rate 1.4 mm/min. X axis is the distance from the center axis and Y axis is the height of interface. In case 1, for the purpose of satisfied crystal quality, the average pulling rate is 1.4 mm/min. Further enhance the pulling speed may cause more defects which can lower the quality of crystal. While for case 2 and 3, when the crystal position is 100, the interface is nearly flat in center, but it concaves down at the edge of interface. For other crystal positions, the interface is seriously concave up near the center axis and slightly concave down at the edge of the crystal. So the cooling jacket has a significant effect on the shape of melt/crystal interface.

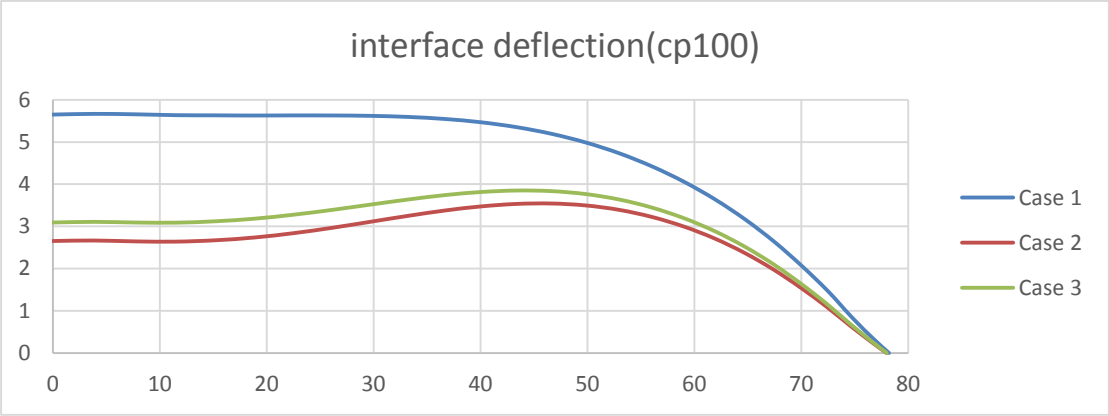

Figure 27 melt/crystal interface deflection for three cases at crystal position 100.

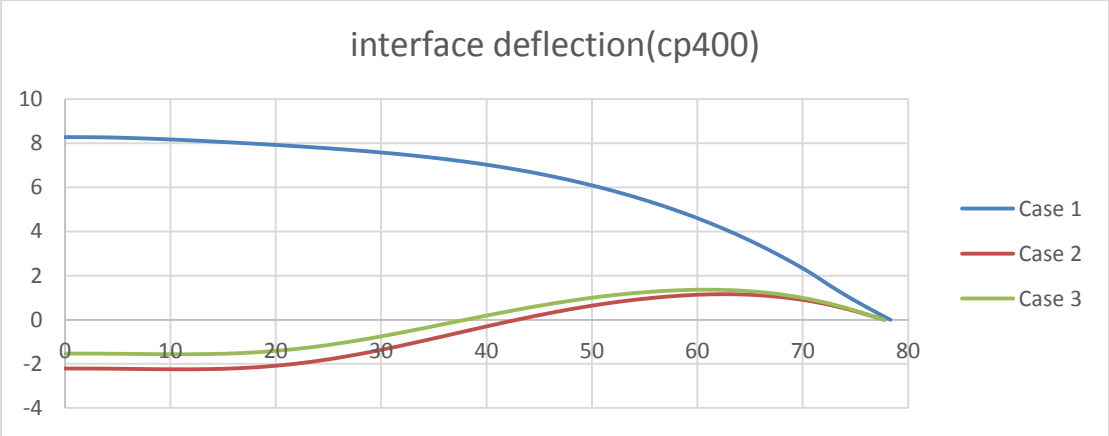

Figure 28 melt/crystal interface deflection for three cases at crystal position 400.

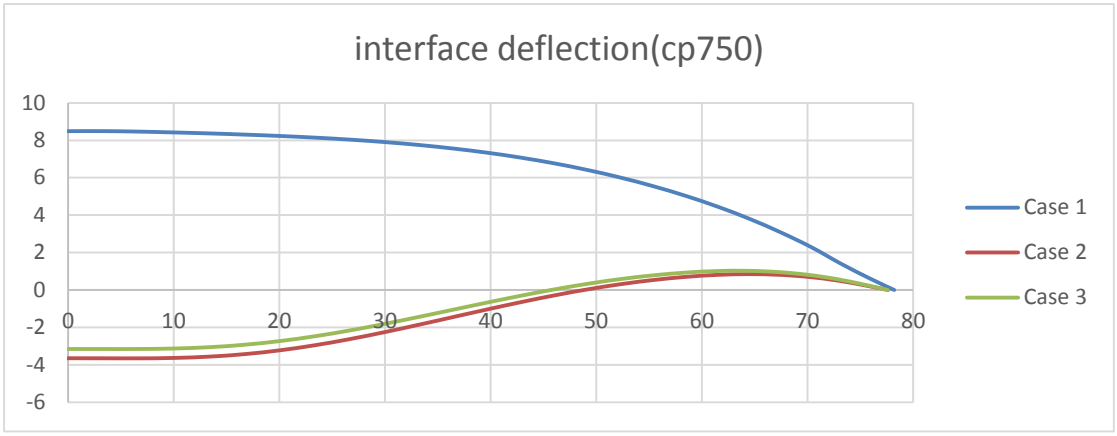

Figure 29 melt/crystal interface deflection for three cases at crystal position 750.

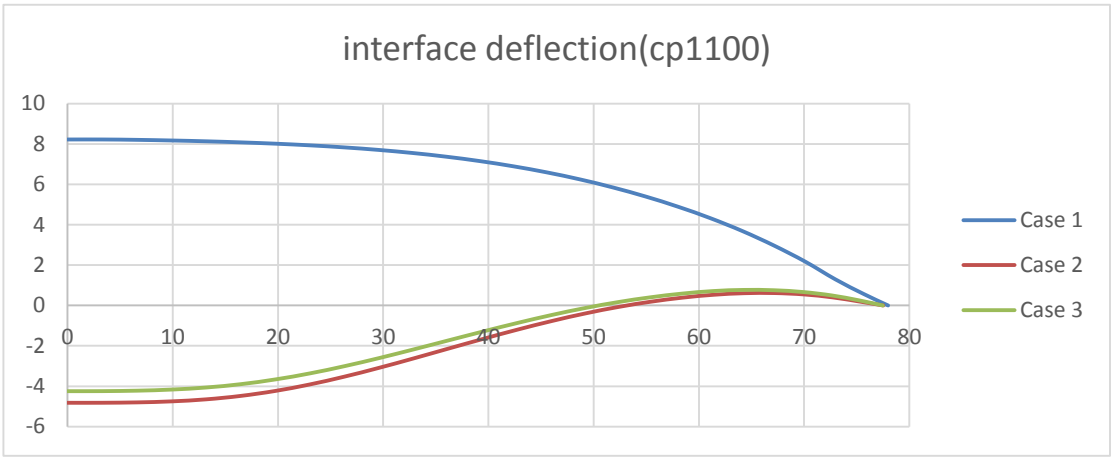

Figure 30 melt/crystal interface deflection for three cases at crystal position 1100.

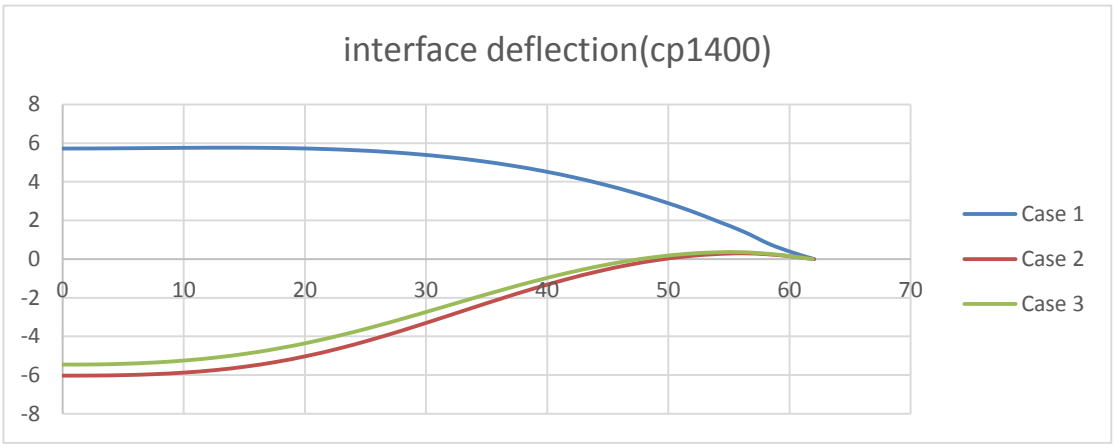

Figure 31 melt/crystal interface deflection for three cases at crystal position 1400.

5 Comparison for different pulling rate

In order to compare the different modifications of the furnace, it was decided to use case 1 wihh pull rate 1.4mm/min and an interface deflection of 8 mm as the standard case to compare against. With the increasing pull rate of case 2 and case 3, the solid-liquid interface deflection will have a corresponding change. As an example of crystal position 750, Figure 32 and Figure 33 show the interface deflection of two cases at pull rate 1.4, 1.6, 1.8 2.0 and 2.2 mm/min, respectively. After installing the cooling jacket, the pull speed can be improved significantly and keep a good crystal quality at the same time. For case 2, the maximum pull rate can reach to 2.2mm/min, for case 3, the maximum pull rate can reach to 2.0mm/min.

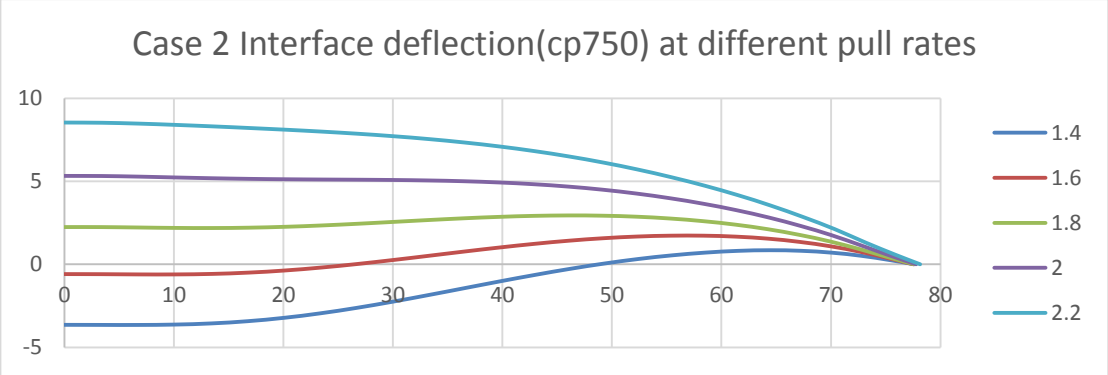

Figure 32 melt/crystal interface deflection at different pull rates (Case 2).

Figure 34 and Figure 35 show the melt free surface temperature at different pull rate (cp750 as an example). It is shown that with the increasing pull rate, the melt free surface temperature will decrease. But if we compare it with the case 1, it is still 5 higher than it. Thus the supercooling can be avoided.

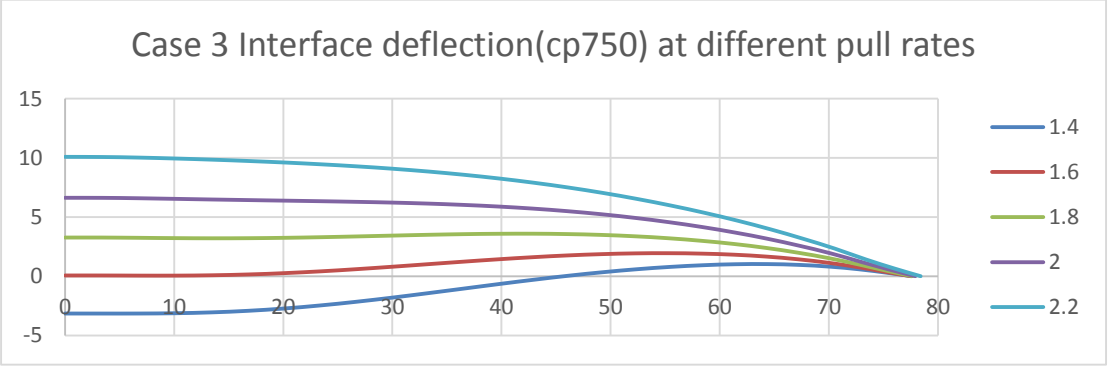

Figure 33 melt/crystal interface deflection at different pull rates (Case 3).

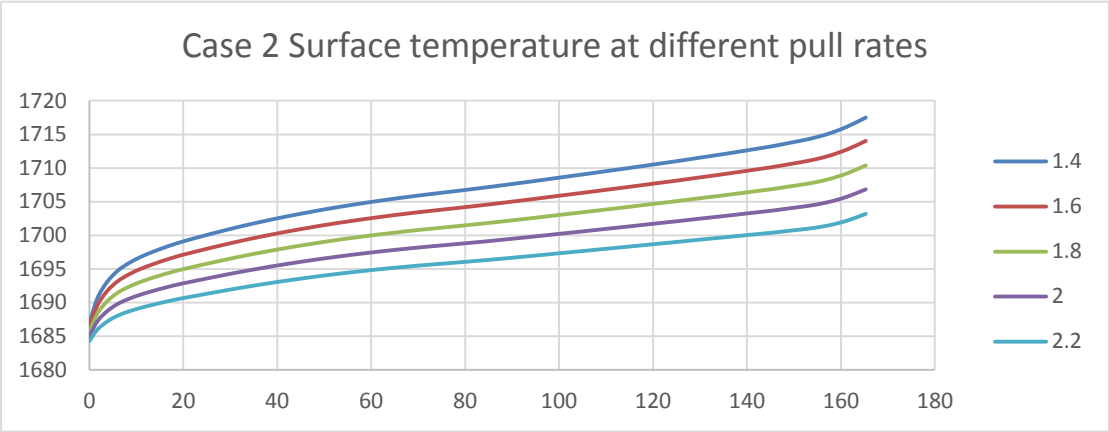

Figure 34 melt free surface temperature at different pull rates (Case 2).

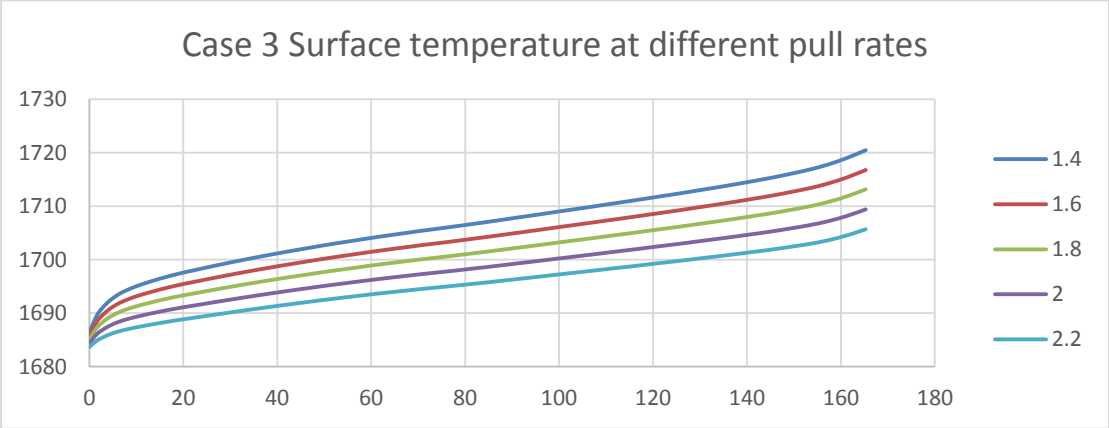

Figure 35 melt free surface temperature at different pull rates (Case 2).

6 Power consumption

The changes of heater power with the crystal height for three cases are shown in Figure 30. Pull rate is set up as 2.2 mm/min, which is 57% higher than case 1 (1.4mm/min). We can see that after installing the cooling jacket, more heat is needed, especially for case 2. The power consumption of case 3 is about 25% higher than case 1. Therefore, the case 2 have a lower power consumption than case 1.

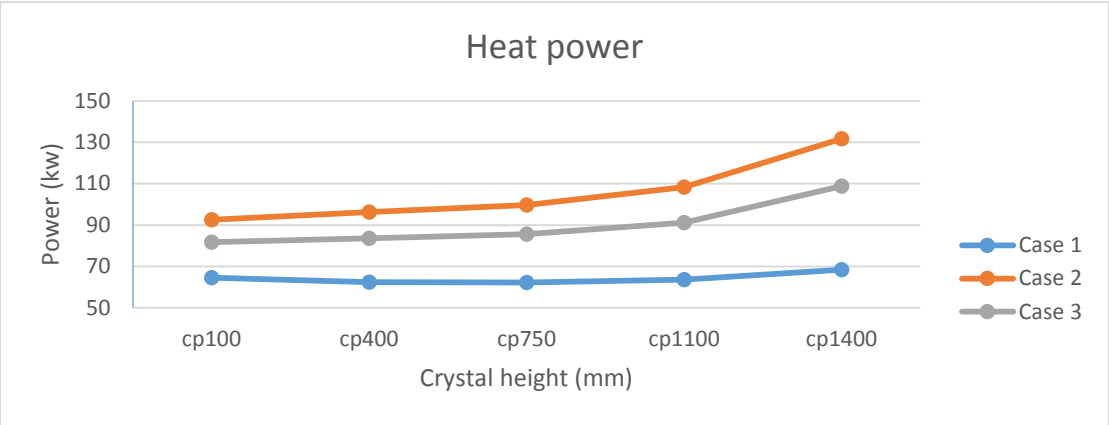

Figure 36 Power consumption at different crystal positions.

7 Defect formation

Two neighboring defect zones have been found in single crystal silicon, which are inner vacancy zone (v) and out interstitial zone (i) respectively. The inner vacancy zone can be further decomposed into the central zone with higher vacancy concentration and the marginal band of lower vacancy concentration, which is distinguished by the oxidization stacking fault ring (OSF-Ring) [24]. OSF-ring is able to decrease the efficiency of solar cell by reducing the minority lifetime.

V/G ratio controls the formation of vacancy zone and interstitial, where V is the growth rate and G is the axial temperature gradient near the interface. To avoid the OSF-ring, the V/G ratio should be higher than the critical value ($C_{critical}$=0.0013-0.002 cm^2/min K) [24]. Figure 37 and Figure 38 show the V/G ratio of case 2 and case 3, when the pull rate is lower than 2 mm/min, the V/G ratio near the edge of crystal are lower than $C_{critical}$=0.0013 cm^2/min K. With the higher pull rates, all V/G ratio are higher than the critical value. Thus, the quality of single crystal can be maintained well at high pull speed.

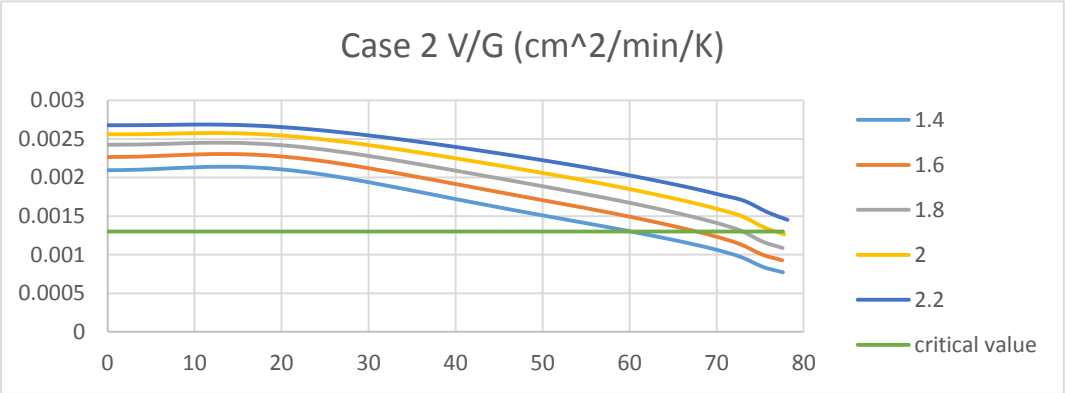

Figure 37 V/G ratio at different pull rate (Case 2).

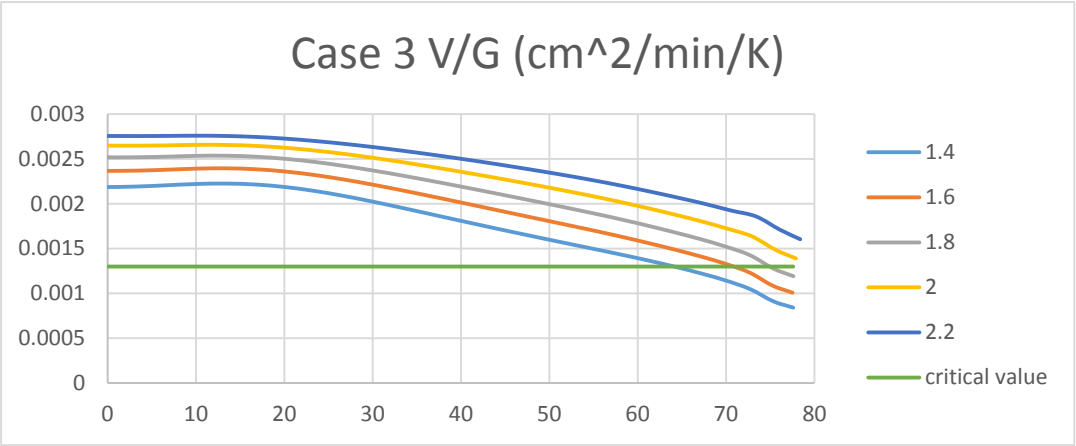

Figure 38 V/G ratio at different pull rate (Case 3).

Chapter 5 Conclusion

In Cz crystal growth, for the purpose of increasing the pull rate, a cooling jacket is installed in the furnace and used water as the cooling medium. We simulated the heat distributions of Case 1, Case 2 and Case 3.

By comparing the results between three cases, we obtained following conclusions:

1. The new cases have flatter isotherm than before, which means the thermal stress can be decreased.
2. After installing the cooling jacket, along the melt/solid interface, the increase of crystal temperature gradient is higher than the increase of melt temperature gradient, thus the pull rate can be increased.
3. The average temperature of melt free surface is higher after installing the cooling jacket, which can avoid the melt supercooling. Besides, the temperature of melt/crucible interface is higher, the oxygen may involve into the melt.
4. The pull rate can be improved obviously, which can increase the productivity.
5. With the increasing pull rate, the V/G ratio are higher than $C_{critical}$=0.0013cm^2/min K, therefore the satisfied single crystal quality can be obtained at high pull rate.
6. The power consumption of the process is lower than before, which is the initial request of simulation.
7. Case 3 shows a better results than case 2 since its lower power consumption and melt/crucible interface temperature.

Chapter 6 Further Work

From the results we can see that after installing the cooling jacket, the melt/crucible interface temperature is higher than before. The reason for this may be that the bottom of cooling jacket is too closed to the melt surface. For the further work, as shown in we plan to set some insulation materials at the bottom of cooling jacket and compare the results with case 2 and case 3.

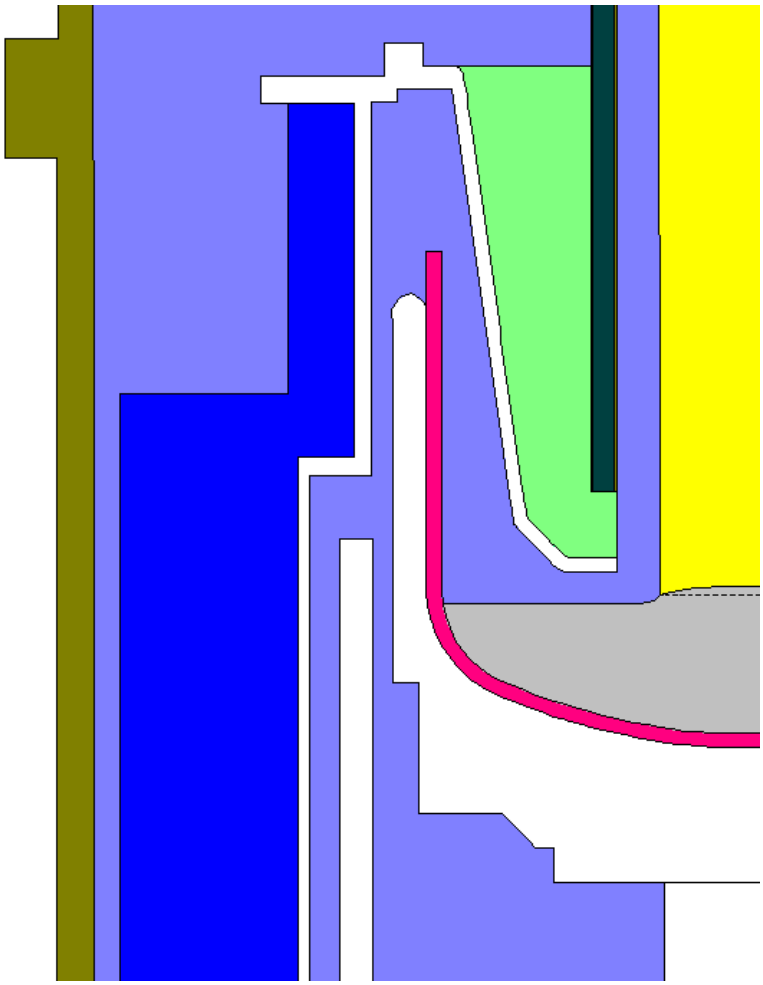

Figure 39 cooling jacket with insulation at the bottom

References

[1] Cutler J. Cleveland and Christopher Morris, Section 15 - Photovoltaics, In Handbook of Energy, edited by Cutler J. Cleveland Christopher Morris, Elsevier, Boston, 2014, Pages 287-302, ISBN 9780124170131.

[2] W.G.J.H.M. van Sark, 1.02 - Introduction to Photovoltaic Technology, In Comprehensive Renewable Energy, edited by Ali Sayigh, Elsevier, Oxford, 2012, Pages 5-11, ISBN 9780080878737.

[3] DOE funds for 'Million Solar Roofs Initiative', Photovoltaics Bulletin, Volume 2003, Issue 7, July 2003, Page 2, ISSN 1473-8325.

[4] M. Tatsuta, New sunshine project and new trend of PV Ramp;D program in Japan, Renewable Energy, Volume 8, Issues 1–4, May–August 1996, Pages 40-43, ISSN 0960-1481.

[5] Bikash Kumar Sahu, A study on global solar PV energy developments and policies with special focus on the top ten solar PV power producing countries, Renewable and Sustainable Energy Reviews, Volume 43, March 2015, Pages 621-634, ISSN 1364-0321.

[6] K. Branker, M.J.M. Pathak, J.M. Pearce, A review of solar photovoltaic levelized cost of electricity, Renewable and Sustainable Energy Reviews, Volume 15, Issue 9, December 2011, Pages 4470-4482, ISSN 1364-0321.

[7] Joshua M Pearce, Photovoltaics — a path to sustainable futures, Futures, Volume 34, Issue 7, September 2002, Pages 663-674, ISSN 0016-3287.

[8] B. Fickett, G. Mihalik, Multiple batch recharging for industrial CZ silicon growth, Journal of Crystal Growth, Volume 225, Issues 2–4, May 2001, Pages 580-585, ISSN 0022-0248.

[9] I.Yu. Evstratov, V.V. Kalaev, A.I. Zhmakin, Yu.N. Makarov, A.G. Abramov, N.G. Ivanov, A.B. Korsakov, E.M. Smirnov, E. Dornberger, J. Virbulis, E. Tomzig, W. von Ammon, Numerical study of 3D unsteady melt convection during industrial-scale CZ Si-crystal growth, Journal of Crystal Growth, Volumes 237–239, Part 3, April 2002, Pages 1757-1761, ISSN 0022-0248.

[10] Bok-Cheol Sim, Yo-Han Jung, Jai-Eun Lee, Hong-Woo Lee, Effect of the crystal–melt interface on the grown-in defects in silicon CZ growth, Journal of Crystal Growth, Volume 299, Issue 1, 1 February 2007, Pages 152-157, ISSN 0022-0248.

[11] L. Suganthi, Anand A. Samuel, Energy models for demand forecasting—A review, Renewable and Sustainable Energy Reviews, Volume 16, Issue 2, February 2012, Pages 1223-1240, ISSN 1364-0321.

[12] Rainer Hinrichs-Rahlwes, Renewable energy: Paving the way towards sustainable energy security: Lessons learnt from Germany, Renewable Energy, Volume 49, January 2013, Pages 10-14, ISSN 0960-1481.

[13] E. Dornberger, W. von Ammon, N. Van den Bogaert, F. Dupret, Transient computer simulation of a CZ crystal growth process, Journal of Crystal Growth, Volume 166, Issues 1–4, 1 September 1996, Pages 452-457, ISSN 0022-0248.

[14] L.Y. Huang, P.C. Lee, C.K. Hsieh, W.C. Hsu, C.W. Lan, On the hot-zone design of Czochralski silicon growth for photovoltaic applications, Journal of Crystal Growth, Volume 261, Issue 4, 1 February 2004, Pages 433-443, ISSN 0022-0248.

[15] A. Sabanskis, K. Bergfelds, A. Muiznieks, Th. Schröck, A. Krauze, Crystal shape 2D modeling for transient CZ silicon crystal growth, Journal of Crystal Growth, Volume 377, 15 August 2013, Pages 9-16, ISSN 0022-0248.
[16] X. Geng, X.B. Wu, Z.Y. Guo, Numerical simulation of combined flow in Czochralski crystal growth, Journal of Crystal Growth, Volume 179, Issues 1–2, 1 August 1997, Pages 309-319, ISSN 0022-0248.
[17] V.V. Kalaev, I.Yu. Evstratov, Yu.N. Makarov, Gas flow effect on global heat transport and melt convection in Czochralski silicon growth, Journal of Crystal Growth, Volume 249, Issues 1–2, February 2003, Pages 87-99, ISSN 0022-0248.
[18] Yutaka Shiraishi, Susumu Maeda, Kozo Nakamura, Prediction of solid–liquid interface shape during CZ Si crystal growth using experimental and global simulation, Journal of Crystal Growth, Volume 266, Issues 1–3, 15 May 2004, Pages 28-33, ISSN 0022-0248,
[19] W.C. Dash, Growth of silicon crystals free from dislocations, J. Appl. Phys. 30(1959)459.
[20] Olli Anttila, Chapter Two - Czochralski Growth of Silicon Crystals, In Micro and Nano Technologies, edited by Veikko Lindroos, Markku Tilli, Ari Lehto and Teruaki Motooka, William Andrew Publishing, Boston, 2010, Pages 19-36, Handbook of Silicon Based MEMS Materials and Technologies, ISBN 9780815515944.
[21] Wenjia Su, Ran Zuo, Kirill Mazaev, Vladimir Kalaev, Optimization of crystal growth by changes of flow guide, radiation shield and sidewall insulation in Cz Si furnace, Journal of Crystal Growth, Volume 312, Issue 4, 1 February 2010, Pages 495-501, ISSN 0022-0248.
[22] P Hopfgartner, P Collareta, M Porrini, Thermal history simulation of Czochralski silicon crystals and its application to the study of defects formation during crystal growth, Materials Science and Engineering: B, Volume 73, Issues 1–3, 3 April 2000, Pages 158-162, ISSN 0921-5107.
[23] George Williams, Raymond E. Reusser, Heat transfer in silicon Czochralski crystal growth, Journal of Crystal Growth, Volume 64, Issue 3, 1 December 1983, Pages 448-460, ISSN 0022-0248.
[24] V.V. Voronkov, R. Falster, Grown-in microdefects, residual vacancies and oxygen precipitation bands in Czochralski silicon, Journal of Crystal Growth, Volume 204, Issue 4, August 1999, Pages 462-474, ISSN 0022-0248.
[25] V.V. Voronkov, Grown-in defects in silicon produced by agglomeration of vacancies and self-interstitials, Journal of Crystal Growth, Volume 310, Issues 7–9, April 2008, Pages 1307-1314, ISSN 0022-0248.
[26] Th. Wetzel, J. Virbulis, A. Muiznieks, W. von Ammon, E. Tomzig, G. Raming, M. Weber, Prediction of the growth interface shape in industrial 300 mm CZ Si crystal growth, Journal of Crystal Growth, Volume 266, Issues 1–3, 15 May 2004, Pages 34-39, ISSN 0022-0248.